Available online at www.sciencedirect.com
SCIENCE DIRECT®
Journal of Hydrology 298 (2004) 80–111
Journal of Hydrology
www.elsevier.com/locate/jhydrol

Preserving high-resolution surface and rainfall data in operational-scale basin hydrology: a fully-distributed physically-based approach

Valeriy Y. Ivanov[a,b,*], Enrique R. Vivoni[a,c,1], Rafael L. Bras[a,d,2], Dara Entekhabi[a,e,3]

[a]*Ralph M. Parsons Laboratory, Department of Civil and Environmental Engineering, Massachusetts Institute of Technology, Cambridge, MA 02139, USA*
[b]*Department of Civil and Environmental Engineering, Massachusetts Institute of Technology, 77 Massachusetts Ave., Room 48-212, Cambridge, MA 02139, USA*
[c]*Department of Earth and Environmental Science, New Mexico Institute of Technology, 801 Leroy Place, MSEC 244, Socorro, NM 87801, USA*
[d]*Department of Civil and Environmental Engineering, Massachusetts Institute of Technology, 77 Massachusetts Ave., Room 48-211, Cambridge, MA 02139, USA*
[e]*Department of Civil and Environmental Engineering, Massachusetts Institute of Technology, 77 Massachusetts Ave., Room 48-331, Cambridge, MA 02139, USA*

Received 14 May 2003; revised 30 October 2003; accepted 29 March 2004

Abstract

This study presents various aspects of the continuous simulation capabilities of a fully-distributed, triangulated irregular network (TIN) hydrologic model. The TIN-based Real-time Integrated Basin Simulator (tRIBS) is calibrated and verified for the Baron Fork at Eldon, Illinois River at Watts, and Blue River at Blue over the period 1993–2000. Computational effort is significantly reduced by simulating complex watersheds using a multiple resolution mesh to represent terrain. Model performance is assessed by comparing streamflow predictions to observations at the basin outlet and interior gauging stations. In addition, simulation results describing the distributed basin response to atmospheric forcing are discussed, including the spatial and temporal variability of runoff, surface soil moisture, evaporative flux, and groundwater table position. By modeling the land-surface water and energy states and fluxes over the computational domain in an efficient manner, the potential for utilizing fully-distributed models at the scales of operational hydrologic forecasting is realized. Through the spatially-explicit approach, high-resolution remote sensing data describing surface properties, topography, rainfall, and soil moisture can be

* Corresponding author. Address: Department of Civil and Environmental Engineering, Massachusetts Institute of Technology, 77 Massachusetts Ave., Room 48-208, Cambridge, MA 02139, USA. Tel.: +1-617-253-1969; fax: +1-617-253-7475.
E-mail addresses: viva@mit.edu (V.Y. Ivanov), vivoni@nmt.edu (E.R. Vivoni), rlbras@mit.edu (R.L. Bras), darae@mit.edu (D. Entekhabi).
[1] Tel.: +1-505-835-5611; fax: +1-505-835-6436.
[2] Tel.: +1-617-253-2117; fax: +1-617-258-8850.
[3] Tel.: +1-617-253-9698; fax: +1-617-253-7475.

doi:10.1016/j.jhydrol.2004.03.041

integrated directly into a predictive hydrologic model. A greater degree of physical interpretation of hydrological estimation can thus be added to existing methods of operational forecasting.

Keywords: Distributed hydrological model; Runoff generation; Streamflow; Triangulated irregular network (TIN); Multiple resolution; DMIP

1. Introduction

The current generation of operational hydrological models lag in the use of information describing the interior watershed structure and in the representation of processes in a spatially distributed form. Although many commonly used models use efficient conceptual frameworks and have extensive operational use (e.g. Schaake et al., 1996; Finnerty et al., 1997; Koren et al., 1999), they ignore the important spatial dynamics of the hydrologic components. Such frameworks commonly emphasize only the integrated behavior of the hydrologic system, in particular, the outlet streamflow hydrograph. While the basin lumped response is important for characterizing the hydrologic regime at the catchment outlet, new challenges imposed by society and changing environmental conditions cannot be satisfied without considering the interior basin response. Spatiotemporal dynamics of precipitation fields, surface soil moisture, and channel discharge as well as catchment topography and soil attributes are the key factors impacting our ability to predict the timing and magnitude of streamflow events (e.g. Pessoa et al., 1993; Goodrich et al., 1995; Wooldridge et al., 2001). Spatial heterogeneity of topography, landuse, vegetation stand, and fine-scale dynamics of soil moisture are also among the major predictors of landslide and fire occurrence (e.g. Pelletier et al., 1997; Bogaard and Van Asch, 2002; Taylor and Solem, 2001). In addition, sustainable management of natural resources relies on information about characteristic catchment properties, such as the tendency to accumulate or drain moisture in/from certain sites which is critical for ecosystem and habitat quality (e.g. Poiani and Johnson, 1993).

Fully-distributed hydrologic models, i.e. those that are capable of resolving variability in hydrologic response of the interconnected hillslope system arising due to soils and topography effects on subsurface lateral water redistribution, attempt to explicitly represent catchment and hydrometeorologic spatial non-uniformity. While a variety of such models exists (e.g. Abbott et al., 1986a,b; Beven et al., 1987; Grayson et al., 1992; Julien and Saghafian, 1991; Wigmosta et al., 1994; Garrote and Bras, 1995; Berger and Entekhabi, 2001), spatially explicit frameworks have yet to become the conventional tool for operational hydrology (Finnerty et al., 1997). Although there is a compelling need for these methodologies, difficulties in parameterization and the associated computational costs for such approaches so far have been prohibitively high. Execution times have to be minimized in order to (1) make feasible distributed model calibrations, (2) perform ensemble averaging of the model results to incorporate uncertainties in model forcing and parameterizations, (3) conduct real-time operational forecasting with distributed hydrologic models. One possible approach is simplifying the modeled hydrological processes and representing the key catchment attributes, such as topography, soils, landuse, and drainage network, in some skillful manner.

The present study points to new avenues for utilizing a physically-based, fully-distributed watershed model at the scales that are of primary interest to operational hydrology (the model itself is not operational). To make such applications computationally feasible, the model employs an irregular spatial discretization in representing river basins. Use of a multiple resolution approach, triangulated irregular networks (TINs) in particular, provides the flexibility required for treating large watersheds efficiently, thus capturing the basin hydrologic features with only 5–10% of the nodes used by regular grid models (Vivoni et al., 2004). The presented study outlines various aspects of the continuous hydrologic simulation of mid-to-large scale National Weather Service (NWS) operational watersheds in Oklahoma and Arkansas (800–1600 km^2) within the framework of the Distributed Model Intercomparison Project (DMIP). The model framework, its capabilities for explicit spatial

modelling as well as a manual calibration methodology are discussed. In the presented examples, the value of the distributed approach is addressed for a variety of temporal and spatial scales. Derived characteristic relationships for the mean long-term values of the key state variables, such as soil moisture, runoff generation, and groundwater table depth, illustrate how terrain, soils, and landuse control the catchment hydrologic regimes.

2. Outline of the model

2.1. Hydrological processes description

The *TIN-based real-time integrated basin simulator* (tRIBS) is the hydrological model used in this study. The model stresses the role of topography in lateral soil moisture redistribution accounting for the effects of heterogeneous and anisotropic soil. An adaptive multiple resolution approach, discussed by Vivoni et al. (2004), is used to represent the complexity of the simulation domain. The model explicitly considers spatial variability in precipitation fields, land-surface descriptors and is capable of resolving basin hydrologic response at very fine temporal (hourly) and spatial (10–100 m) scales. tRIBS includes parameterizations of rainfall interception, evapotranspiration, infiltration with continuous soil moisture accounting, lateral moisture transfer in the unsaturated and saturated zones, and runoff routing. The model computational basis, structure, and description of processes parameterizations are given in full detail in Ivanov et al. (2004) who also provide a few illustrative examples of the model capabilities based on the results of the first phase of DMIP (see Smith et al., this issue). However, the work focuses on model performance and does not duplicate the development of Ivanov et al. (2004). To familiarize the reader with the hydrological functionality of tRIBS, an outline of the process parameterizations implemented in the model is given below.

2.1.1. Precipitation interception

The Rutter canopy water balance model (Rutter et al., 1971, 1975) is used. Canopy water dynamics is species dependent such that the parameters vary for different vegetation types.

2.1.2. Surface energy model

Short wave and long wave radiation components are simulated accounting for geographic location, time of year, aspect and slope of the element surface (Bras, 1990). The combination equation (Penman, 1948; Monteith, 1965), gradient method (Entekhabi, 2000), and force-restore (Lin, 1980; Hu and Islam, 1995) method are used to estimate the latent, sensible, and ground heat fluxes at the land-surface. An optimum is sought in terms of the soil surface temperature that leads to the energy balance. Soil water content in the root zone and top soil layer constrains evapotranspiration from vegetated surfaces and bare soil. A species-dependent parameterization of stomatal conductance allows for diurnal variation of transpiration flux.

2.1.3. Evapotranspiration partition

Depending on vegetation fractional coverage of an element and canopy state, latent heat energy is partitioned into vegetation transpiration, bare soil evaporation, and evaporation from the wet canopy.

2.1.4. Infiltration

Parameterization of the process involves the assumption of gravity-dominated flow in heterogeneous, anisotropic soil. Evolution of the wetting front and top front in an element may lead to unsaturated, perched, surface, and completely saturated states. The unsaturated and the saturated zones are coupled, accounting for the interaction of the moving infiltration front with a variable groundwater table. Topography and soil control the magnitude of the lateral moisture transfer in the unsaturated zone. Continuous soil moisture accounting allows for handling both storm and interstorm periods thus permitting long-term simulation over a range of hydrometeorological forcings.

2.1.5. Groundwater

A quasi three-dimensional ‘cascade’ groundwater model allows for lateral water redistribution in the saturated zone and dynamic interaction with the unsaturated zone.

2.1.6. Runoff production

Runoff generation is made possible via a variety of mechanisms: saturation excess, infiltration excess,

perched subsurface stormflow, and groundwater exfiltration.

2.1.7. Overland flow

Non-linear hydrologic routing relates overland flow velocities to a local stream discharge value. A re-infiltration scheme is not considered in the model.

2.1.8. Channel flow

Kinematic wave routing is used to model water transport and dispersion in natural channels whose geometry is defined through geomorphic relationships or channel cross section measurements.

Numerical schemes use an efficient finite-difference control-volume approach to solve the governing equations using Voronoi polygons as basic computational units (Ivanov et al., 2004). The maximum slope direction is chosen to construct the drainage network for overland flow routing across a watershed terrain as well as to simulate subsurface mass flux interchange between the contiguous cells. Stream channels are pre-defined by using the network extracted from the DEM. Explicitly accounting for the local dynamics and lateral mass exchanges, the model is capable of producing the spatially distributed hydrologic response of a catchment.

2.2. Simulation capabilities and model output

The tRIBS model provides outputs ranging over a variety of spatial and temporal scales.

2.2.1. Point scale

At the smallest spatial scale, the Voronoi element, evolution of all the hydrological state variables can be obtained: rainfall interception, evaporation from the canopy, evolution of the infiltration fronts, dynamics of subsurface fluxes in the unsaturated and saturated zones, soil moisture conditions, runoff generation, and evapotranspiration. Analysis of these dynamics is extremely important for verifying the general physical soundness of the model performance as well as for calibrating parameters of certain hydrological processes (see Section 4.1).

2.2.2. Hillslope transect scale

A group of Voronoi cells forming a hillslope transect can be selected based on the drainage directions connecting the contiguous cells. Time-varying cross-sectional profiles of the hydrological variables can thus be obtained. If field or experimental information about temporal dynamics of the soil moisture and groundwater along the hillslope is available, the pertinent model parameters can be adjusted.

2.2.3. River reach scale

The catchment channel network can be represented with a sufficiently high accuracy by a union of segments connecting the stream nodes (Vivoni et al., 2004). For each node of the channel network, the time-series of streamflow are provided. This offers the flexibility of tracking the spatial variability of runoff conditions in the catchment. As opposed to semi-distributed modelling approaches that pre-define points of interest by partitioning the main catchment into nested sub-basins, the approach in tRIBS provides hydrologic prediction at any point of the channel network.

2.2.4. Basin scale

The capability for reproducing internal variation of hydrologic response is among the essential features offered by distributed models. Spatial fields of state variables, for example, such as soil moisture, are amenable for use with remote sensing data (Hoeben and Troch, 2000; Schmugge et al., 2002; Walker et al., 2002), a promising direction in model calibration (e.g. Grayson and Bloschl, 2000; Refsgaard, 2000; Pauwels et al., 2001). tRIBS produces spatial maps of all the major hydrological state variables (energy and water fluxes, canopy state, soil moisture conditions, runoff generation, etc.) at a specified temporal resolution. In addition to instantaneous basin states, the model generates frequency distributions and their moments for a number of hydrological variables, thus providing integral representation of site specific properties.

3. Preserving the spatial variability of basin attributes and hydrometeorologic input

3.1. Test basins

Three test basins were used in the following the DMIP modeling exercises: Baron Fork at Eldon,

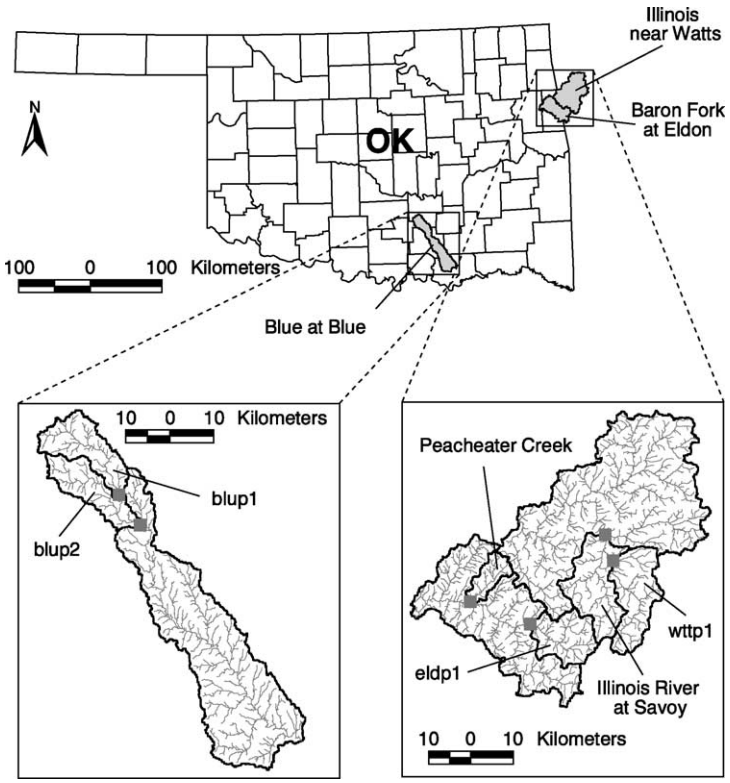

Fig. 1. Location of the test watersheds: Blue River, Baron Fork, and Illinois River near Watts basins. Nested locations are depicted as shaded squares.

Blue River at Blue, and Illinois River near Watts. For each of these watersheds, two nested locations were provided for which streamflow simulations were performed (Fig. 1). Basic topographic and hydrologic characteristics for these catchments and their nested sub-basins are summarized in Table 1, based on Slack et al. (2001), USGS streamflow, and USGS DEM data (see also Smith et al., this issue). The following is a general description of terrain, soil, and landuse features in the catchments.

The terrain of the Baron Fork watershed is characterized by gently rolling relief at the basin headwaters and quite rugged terrain in its lower areas. The sub-basins corresponding to two nested locations have diverse topographies with significant slopes of the channel network. The watershed contains two nested gaged locations (Table 1). The simulations were conducted for one of them—Peacheater Creek at Christie. The Baron Fork watershed has significant vegetation cover: about 52% of the area is occupied by deciduous and evergreen forests, 46% is occupied by croplands and orchards. The surface soil texture is primarily silt loam (94%) and fine sandy loam (6%).

The Illinois River near Watts catchment is located just north from the Baron Fork watershed and has similar topographic characteristics: flatter areas in the upstream region with more rugged terrain in the center of the watershed and downstream regions. Among the two nested sub-basins, one is instrumented with a streamflow gage (Table 1). Croplands and pastures occupy about 65% of the watershed area, about 28% is occupied by forests which are dominated by deciduous trees. The watershed is almost unurbanized (about 6%). The dominant soil type is loam.

The terrain of the Blue River basin is characterized by low relief along the whole course of the river. The gently sloping channels are deeply incised. The woody savanna is the dominant type of vegetation (about 77%), deciduous forests occupy about 14% of the catchment area, the rest of the catchment is

Table 1
Basic topographic and hydrologic characteristics of the test basins

Basin/USGS gauge#	A (km^2)	H/C_{vH} (m)/(–)	L (km)	S_L (m/km)	S_A (m/km)	P (mm)	Q (mm)/(cm)
Baron Fork at Eldon (USGS 0719700)	800	346/0.462	65.2	4.35	15.3	1130	371/9.43
Sub-basin Peacheater Creek at Christie (USGS 07196973)	64	328/0.352	18.1	6.74	11.7		368/0.75
Sub-basin Baron Fork at Dutch Mills (*not used in DMIP*) (USGS 07196900)	105	408/0.559	17.8	8.26	20.8		388/1.29
Sub-basin(*eldp1*) ungaged location	152	395/0.508	25.0	6.86	20.0		
Illinois river near watts (USGS 07195500)	1640	378/0.402	75	2.3	10.8	1100	346/18.0
Sub-basin(*wttp1*) Ungaged location	210	406/0.681	30.5	5.56	12.2		
Sub-basin Illinois River at Savoy (USGS 07194800)	432	397/0.642	38.9	4.66	12.0		296/4.05
Blue River at Blue (USGS 07332500)	1230	260/0.657	136	1.67	5.28	1000	235/9.20
Sub-basin(*blup1*) ungaged location	171	360/0.411	33.8	2.02	5.11		
Sub-basin(*blup2*) ungaged location	321	354/0.323	47.5	2.09	4.97		

A, basin drainage area; H, basin mean elevation ((m) above NGVD29); C_{vH}, coefficient of variation of elevation as a ratio of standard deviation to the difference between the mean and minimum elevation of the basin; L, maximum distance of channel flow; S_L, average slope of the longest channel; S_A, average slope of channel drainage network; P, mean annual precipitation; Q, mean annual flow.

occupied by evergreen needleleaf forests (about 4–5%), and grasslands and croplands (about 4%). The watershed has an insignificant proportion of urbanized areas: less than 0.5% of the area. There are seven soil types defined in the Blue River catchment with about 53% of the area occupied by loam and silty loam soil type, 16% by fine sandy loam, and 14% by clay.

3.2. Spatial variability of basin land-surface characteristics

There are several land-surface characteristics that need to be explicitly accounted for while describing the interior watershed structure: topography, land-use/vegetation and soils. To represent these catchment properties in the computational domain, the tRIBS model employs an irregular spatial discretization based on TINs. Topography for the test basins was derived from USGS 30 m DEM using the hydrographic TIN procedure described in Vivoni et al. (2004). The approach provides high resolution in areas with significant elevation gradient. River floodplains, resolved at a high detail, were also integrated into the TIN terrain models. Through the TIN implementation, the quantity of computational elements was significantly reduced. Compared to the 30 m resolution DEM, the amount of computational elements for the Baron Fork watershed was 7.22% (64,836 nodes), for Illinois River near Watts—3.98% (72,052 nodes), and for Blue River—3.32% (45,659 nodes) of the original number of grid cells. The equivalent grid cell sizes, i.e. the pixel size in the grids with the same number of computational elements, for these basins are correspondingly 112, 150, and 165 m. A comparative analysis of the TIN accuracy relative to the highest DEM available was conducted by Vivoni et al. (2004).

Information about landuse, vegetation cover, and soils is required for proper parameterization of energy and water fluxes at the land-surface. Spatial heterogeneity of these properties in tRIBS is accounted for by assigning the relevant landuse/soil texture type to the nodes of the computational domain. International Geosphere-Biosphere Program (IGBP) vegetation and the Soil Conservation Service (SCS) State Soil Geographic Database (STATSGO) soils data were used to characterize the Blue River basin. The USGS Land Use and Land Cover (LULC) data were used in the current study to represent landuse and vegetation cover for Baron Fork and Illinois River catchments (Fig. 2). Since the STATSGO data showed essentially homogeneous soil texture types for the two latter watersheds, an alternative approach was chosen to represent spatial non-uniformity of soil hydraulic properties that can affect the infiltration regime. Vegetation and landuse classes were combined to define grassy, forested, and urbanized sites that were

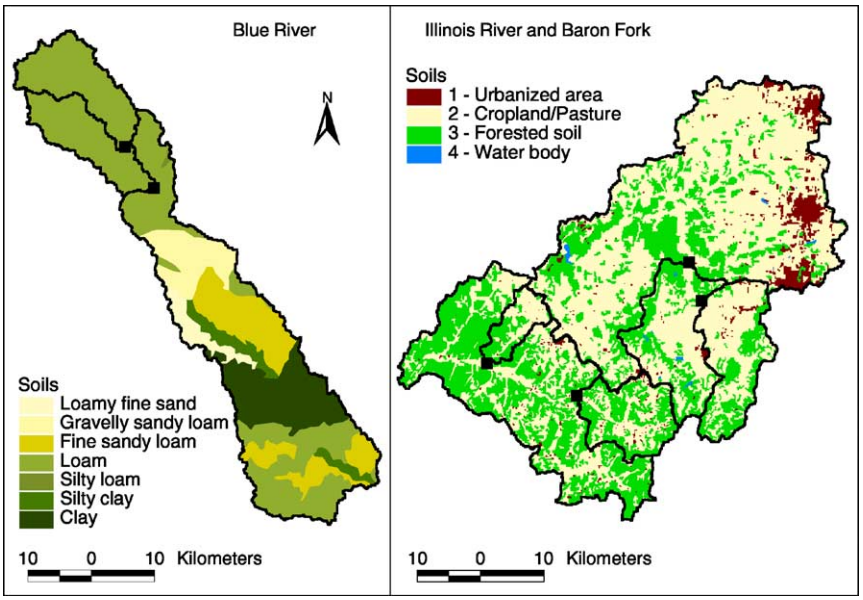

Fig. 2. Soils coverages of Blue River, Baron Fork, and Illinois River near Watts basins used in DMIP simulations.

used as a surrogate representation of soils spatial variability (Fig. 2).

3.3. Drainage networks and channel geometry

Overland drainage networks were constructed from the TIN following Tucker et al. (2001). In general, the steepest edge connected to a given node is used to route the surface flow so that the hillslope flow pathways are completely defined by the catchment TIN. The channel network for each of the basins was pre-defined in the input mesh by explicitly specifying stream nodes corresponding to the DEM-derived channel network (Ivanov et al., 2004). In order to run the hydraulic flow routing model, the channel geometry at all points of the network must be known. While 14 cross-section measurements were provided for the main channel of the Blue River basin (Smith et al., this issue), no information was available for the tributaries as well as for the channels of Baron Fork and Illinois River basins. Regional geomorphological relationships (Leopold and Maddock, 1953) were used to estimate the widths of approximated rectangular cross-sections for these channels. Values of the parameters for all basins were taken from Carpenter et al. (2001).

3.4. Variability of precipitation and hydrometeorologic input

Precipitation spatial variability is one of the major factors affecting non-uniformity of the timing and magnitude of streamflow events in large watersheds (Koren et al., 1999). One of the primary reasons for using spatially explicit modelling approaches is to take advantage of the spatial and temporal resolution in rainfall afforded by weather radars (e.g. Wyss et al., 1990; Pessoa et al., 1993). Since the characteristic size of tRIBS elements is typically of the order of 30–500 m, the model is capable of utilizing the currently available radar products at a fine resolution. In the present study, simulations were driven with radar rainfall estimates from the NWS Next-Generation Weather Radar (NEXRAD) system (for description, see Smith et al., this issue). Processing of weather radar data from the Arkansas-Red River Forecasting Center (ABRFC) for the 1993–2001 period consisted of coordinate transformations from the HRAP to the UTM coordinate system, selection of data corresponding to the geographic extent of a watershed and formatting for model input. tRIBS utilizes an ASCII grid definition for spatial data input (ESRI, 1992). Input of a precipitation grid occurs

during simulation phase when the time tag of the simulation time precedes by 1 h the time tag of the next input NEXRAD rainfall file. A procedure of rainfall data mapping onto irregular elements of the model computational domain then follows (for details see Ivanov et al., 2004).

In addition to radar estimates, the meteorological conditions in a watershed are important descriptors of the evaporative potential. Hourly meteorological data: air and dew point temperature, cloudiness, wind speed, and atmospheric pressure (see Smith et al., this issue) were utilized in tRIBS to compute the surface energy fluxes and evaporation potential. For each basin, a location associated with the catchment center was chosen to obtain the corresponding grid values of the hydrometeorological variables. The files containing input hydrometeorological variables were inputted into the model at the beginning of simulations. During simulations, every time when the evapotranspiration routine was called, a built-in resampling procedure retrieved values from the input arrays and assigned them to the nodes of the catchment TIN.

4. tRIBS calibration methodology

One of the advantages that physically-based approaches offer is that representative parameter values can be obtained directly from measurements or field observations. Nonetheless, in order to obtain adequate simulation results, some of the model parameters require subsequent calibration. Commonly, model performance is measured through comparisons to the discharge at the catchment outlet. Distributed models, however, provide the advantage of representing catchment internal dynamics which allow one to obtain the spatial fields of the state variables of the system. Model skill metrics that capture spatial simulation capabilities can thus be addressed (Grayson and Bloschl, 2000; Refsgaard, 2000).

The following sections provide a general description of the manual calibration methodology of the tRIBS model that was used in the DMIP modelling exercise. The methodology first introduces various parameter groups and ranks these according to importance for model calibration. The sensitivity of components of the hydrologic system is used to identify key parameters that significantly affect rainfall partition and subsurface moisture dynamics. Various spatiotemporal scales of model calibration are subsequently described.

A note has to be made concerning DMIP calibration stipulations. One of the imposed requirements of the DMIP project, which authors of this paper disagree with, was to only use the outlet streamflow hydrographs in model calibration. Therefore all available streamflow records for nested locations (Table 1) for the specified period (see Smith et al., this issue), 06/1993–07/1999 were neglected. While Section 4.2 refers to the calibration of nested sub-basins, it was not performed in this DMIP case study and is provided in the following for purposes of generality only.

4.1. Parameter groups and their relative importance

The tRIBS model parameters are given in Table 2 (which should be used while reading the following) while the relevant hydrologic expressions are provided by Ivanov et al. (2004). The parameters are divided into several groups according to the simulated processes. Different techniques and various simulation time scales are used to adjust parameters and obtain the desired model performance.

While streamflow at the catchment outlet characterizes the model ability to reproduce an integral catchment response, a physically sound hydrological model must realistically simulate the pertinent processes at the elementary scale. tRIBS resolves mass and momentum equations at fine temporal ($\sim$4 min) and spatial (30–500 m) scales thus using physically meaningful parameters that have quite narrow plausible ranges. Some of the parameters are fixed with values obtained from the literature and extensive calibration is performed only for a limited number of parameters to which the model is the most sensitive. Therefore, one may regard the following as a ‘constrained’ calibration.

(1) *Vegetation interception* parameters p, S, K, and g affect the storage capacity and dynamics of moisture in the canopy as well as the amount of net precipitation. Initial values are derived based on reported field studies (e.g. Shuttleworth, 1979; Rutter et al., 1975; Schellekens et al., 1999). Calibration is

Table 2
The tRIBS model parameters

Parameter symbol	Description	Units	Calibration effort
Vegetation properties			*Vegetation*
p	Free throughfall coefficient	–	2
S	Canopy capacity	mm	3
K	Canopy drainage rate coefficient	mm h^{-1}	2
g	Canopy drainage exponent	mm^{-1}	2
a	Surface albedo	–	3
H_v	Vegetation height	m	3
K_t	Optical transmission coefficient	–	2
r_s	Canopy average stomatal resistance	s m^{-1}	1
v	Vegetation fraction	–	1
Soils hydraulic and thermal properties			*Soil*
K_{0n}	Saturated hydraulic conductivity	mm h^{-1}	1
θ_s	Saturation soil moisture content	–	3
θ_r	Residual soil moisture content	–	3
λ_o	Pore-size distribution index	–	2
ψ_b	Air entry bubbling pressure	mm	3
f	Conductivity decay parameter	mm^{-1}	1
a_r	Anisotropy ratio	–	1
n	Total porosity	–	3
k_s	Volumetric heat conductivity	J m^{-1} s^{-1} K^{-1}	2
C_s	Soil heat capacity	J m^{-3} K^{-1}	2
Channel and hillslope routing parameters			*Hydrography*
n_e	Manning's channel roughness	–	1
α_B	Channel width-area coefficient	–	2
β_B	Channel width-area exponent	–	2
c_v	Hillslope velocity coefficient	–	1
r	Hillslope velocity exponent	–	1

Note: 1, primary, significant calibration effort; 2, secondary, minor calibration; 3, tertiary, calibration is minor or not conducted.

minimal and is fully based on the analysis of process dynamics at the basic element scale for each vegetation type.

(2) *Soil thermal* properties and *vegetation* parameters k_s, C_s, a, K_t, r_s, v, and H_v define the partitioning of available energy and the magnitude of the latent heat flux and evapotranspiration components (relevant topographic features, i.e. aspect and slope, are computed directly from the TIN). Initial values are derived based on the soil and landuse classification tables reported in the literature. Only K_t, r_s, and v are calibrated to obtain realistic model behavior. The range of their possible values is defined by the vegetation type present in the element. The coefficient K_t is used to regulate the amount of short wave radiation reaching the ground implying adjustments to the amount of energy available for the latent heat flux. The parameter value can be related to the canopy density characteristic. The stomatal resistance parameter r_s is used to control the departure of the transpiration rate from the potential value. The vegetation fraction v implicitly controls the partitioning of the latent heat flux between the processes of transpiration and evaporation from bare soil. Depending on the relative magnitude of both rates, the amount of moisture loss from the system can be controlled.

(3) *Soil hydraulic properties* K_{0n}, f, a_r, θ_s, θ_r, n, λ, and ψ_b control timing and magnitude of runoff production. These are the key model parameters since they determine the state variables of the system (e.g. soil moisture, runoff). Initial values of these parameters are derived from the soil pedo-transfer functions and values reported in field studies

(e.g. Rawls et al., 1982, 1983). Only K_{0n},f, and a_r are calibrated since they are the principal parameters controlling rainfall partitioning and the magnitude of subsurface lateral exchange. The process of calibration of these parameters is mostly based on the outlet streamflow hydrograph and includes several steps corresponding to various flow regimes and different time scales. The parameters K_{0n},f, and a_r are highly interdependent which may result in numerous possible combinations. The following guidelines have to be considered during calibration of these parameters.

(a) Higher values of f result in fast basin response with an abrupt hydrograph recession limb. The higher the value of f, the larger the chance of infiltration excess runoff. Lower f values result in recessions that do not fall as fast and K_{0n} has increasingly more important effect in the soil's response to rainfall. Rainfall events of extreme intensity with the preceding low baseflow periods are best suited for the initial calibration of K_{0n} and f.

(b) High values of f essentially prohibits generation of the groundwater flow due to highly non-linear transmissivity function (see Sivapalan et al., 1987). A trade-off has to be made between parameter effect on rainfall partitioning and saturated zone dynamics.

(c) Both K_{0n} and f control the timing of production of the major runoff volume. When transport time is insignificant (an outlet region) and the saturation excess as well as perched subsurface stormflow is assumed to be the dominant response mechanisms, timing to the streamflow peak is a representative indicator of how fast the subsurface convergence of moisture fluxes occurs. Slow response corresponds to more conductive soils with the larger e-folding depth of saturated conductivity. For instance, a substantial time delay between the rainfall pulse and the observed bulk runoff volume may indicate that higher values of K_{0n} and lower values of f should be chosen.

(d) The anisotropy ratio a_r offers a way of controlling lateral subsurface exchange both in the unsaturated and saturated zones aside from the direct effect of K_{0n} and f. The magnitude of interflow in the system as well as background catchment baseflow are the best indicators in calibration. A prolonged recession flow limb in areas of steep topography indicates lower values of a_r. Higher values of a_r result in faster convergence of subsurface fluxes in the channel network and a larger fraction of interflow in the basin response. Calibration is best performed for the events when perched subsurface stormflow and groundwater runoff production are believed to be the dominant mechanisms in catchment response.

(e) The rate of decrease and magnitude of baseflow during long interstorm periods is a useful indication of values of f and a_r. Rainless winter recession periods with small evapotranspiration potential are suitable for calibration of these parameters. As it has been shown by Sivapalan et al. (1987), who used the same decay function of the saturated conductivity, the gradient of recession flow can be directly related to the parameter f. Rapid decrease in absolute magnitude of the streamflow gradient of the recession limb of the hydrograph and prolonged subsequent periods of slowly changing baseflow may characterize less conductive deeper soil layers. Thus, higher values of f and smaller values of a_r should be chosen. In contrast, prolonged recession flow and rapidly decreasing to negligible values baseflow can be attributed to more conductive soils.

(4) *Routing* parameters c_v, r, n_e, α_B, and β_B control the shape and timing of the storm hydrograph (geometric characteristics of the drainage network, i.e. slope and length of the travel path, are computed directly from the TIN). As long as the problem of runoff routing can be considered as sufficiently independent from the problem of rainfall partition into infiltration and runoff, the parameters of this group can be viewed as independent. They are calibrated only after a sufficient level of confidence is achieved in the values of the preceding parameter groups. Initial values are derived from the values reported in the literature or from relationships based on measurable field quantities (e.g. Carpenter et al., 1999). Parameter n_e, α_B, and β_B, determining channel characteristics, are calibrated by matching the outlet hydrograph for the events when saturation from below and groundwater runoff production are believed to be the dominant mechanisms in basin response. The coefficients c_v and r, controlling overland flow routing are strongly interdependent. Their calibration is performed for storm events when a substantial amount of infiltration excess runoff associated with hillslope locations is produced.

4.2. Calibration spatiotemporal scales

Manual streamflow-based calibration is a stepwise approach that includes analysis of a number of variables considered at different spatial and temporal scales. A general outline of the procedure, constituting the basis of the tRIBS model calibration, follows.

4.2.1. Spatial aspects

Different approaches may exist to account for information from multiple nested gages in calibration. The approach that has been applied with tRIBS (this was not done in results presented here) is to first perform an independent calibration for each nested basin with existing streamflow records. Calibrated values of vegetation and soil parameter groups for the nested basins are then considered to be fixed and subsequent calibration is performed only for ungaged part of the catchment. The calibrated values of the corresponding groups can be used as initial parameter guesses.

4.2.2. Temporal aspects

The following outlines various temporal scales at which calibration for any given basin is conducted. It is assumed that each basin is calibrated independently and that no internal, uncalibrated sub-basins exist (not applicable to the DMIP study).

(a) Streamflow volume for a *single event* is calibrated to obtain the initial estimates of parameters K_{0n},f, and a_r. Events with high rainfall intensities should be used. Baseflow prior to the event is used to guide the choice of appropriate initial conditions as well as soil conductivity and anisotropy. The initial conditions are derived using quasi-steady state approach of Sivapalan et al. (1987) (for details, see Ivanov et al., 2004). A model 'spin-up' period is also used to match the simulated baseflow to pre-event observations. Various parameter sets are used.

(b) If catchment soil characteristics are represented by several texture types, spatial concentration of the rainfall event may dictate the parameters of which soil group are calibrated most during this step. For instance, if the bulk of rainfall precipitates over areas of a particular soil texture, parameters of the corresponding soil group are calibrated most for the considered event. Preliminary calibration of routing parameters is also performed at this stage.

(c) *Several successive events* are simulated in a continuous run for further adjustment of the soil hydraulic and routing parameters. Comparison of the relative magnitudes of different runoff types is done to check the consistency of the model estimates. Events with different dominant response mechanisms and spatial rainfall structures are used to better calibrate the overland and channel routing parameters. Evaluation of the initial values of evapotranspiration parameters is performed. 'Split-sample test' (Klemes, 1986) can be done at this stage.

(d) A *long interstorm period* after the initial period of successful calibration is used to adjust the evapotranspiration parameters.

(e) A *long continuous period* of simulation is used to compare the observed and simulated flows and check the energy and water balance components. It is desirable that such a simulation combines in a continuous run several calibration events as well as events for which model calibration has not yet been performed.

(f) *Intraannual* discharge variability is checked for consistency with the observed records. The fractional

Table 3
Multi-year statistics of streamflow simulation for the test basins for the period 04/1994–07/2000

Basin	PB (%)/ APB (%)	Q_{obs} (CMS)/ Q_{sim} (CMS)	C_{vobs} (−)/ C_{vsim} (−)	RMS (%)/ ARMS (CMS)	R(−)	N_r (−)
Baron Fork at Eldon	−8.1535/49.991	11.02/10.13	2.920/2.028	192.5/21.23	0.763	0.565
Sub-basin Peacheater Creek at Christie	2.5324/65.970	0.6534/0.6699	3.016/3.343	283.7/1.854	0.619	0.116
(Uncalibrated) Illinois River near Watts	−16.480/45.205	19.96/16.67	2.031/1.917	126.2/25.19	0.788	0.614
(Uncalibrated) *Sub-basin* Illinois River at Savoy	4.524/67.695	5.186/5.421	3.673/2.233	235.5/12.21	0.781	0.589
Blue River at Blue	8.4091/66.075	8.927/9.678	2.692/1.692	183.9/16.41	0.733	0.533

PB, APB, percent bias and absolute percent bias; Q_{obs}, Q_{sim}, observed and simulated means of streamflow. $C_v$obs, $C_v$sim, observed and simulated coefficient of variation of streamflow; RMS/ARMS, root mean square, percent RMS error (%) and absolute RMS error (CMS); R, correlation coefficient. N_r, Nash-Sutcliffe coefficient.

composition of the seasonal streamflow based on partitioning into runoff types is analyzed next to further check the simulation consistency.

5. Model performance

The following results demonstrate several aspects of distributed, physically-based modelling of continuous catchment hydrology. A wide range of hydrologic variables integrated over various time and space scales is illustrated. Lumped representation of the basin dynamics, or the streamflow, in many cases is the only available verifiable measure of the model performance (the only one required for use in the DMIP study). The illustrated spatiotemporal fields of state variables offer new means for validating the simulated dynamics. Relationships, derived from

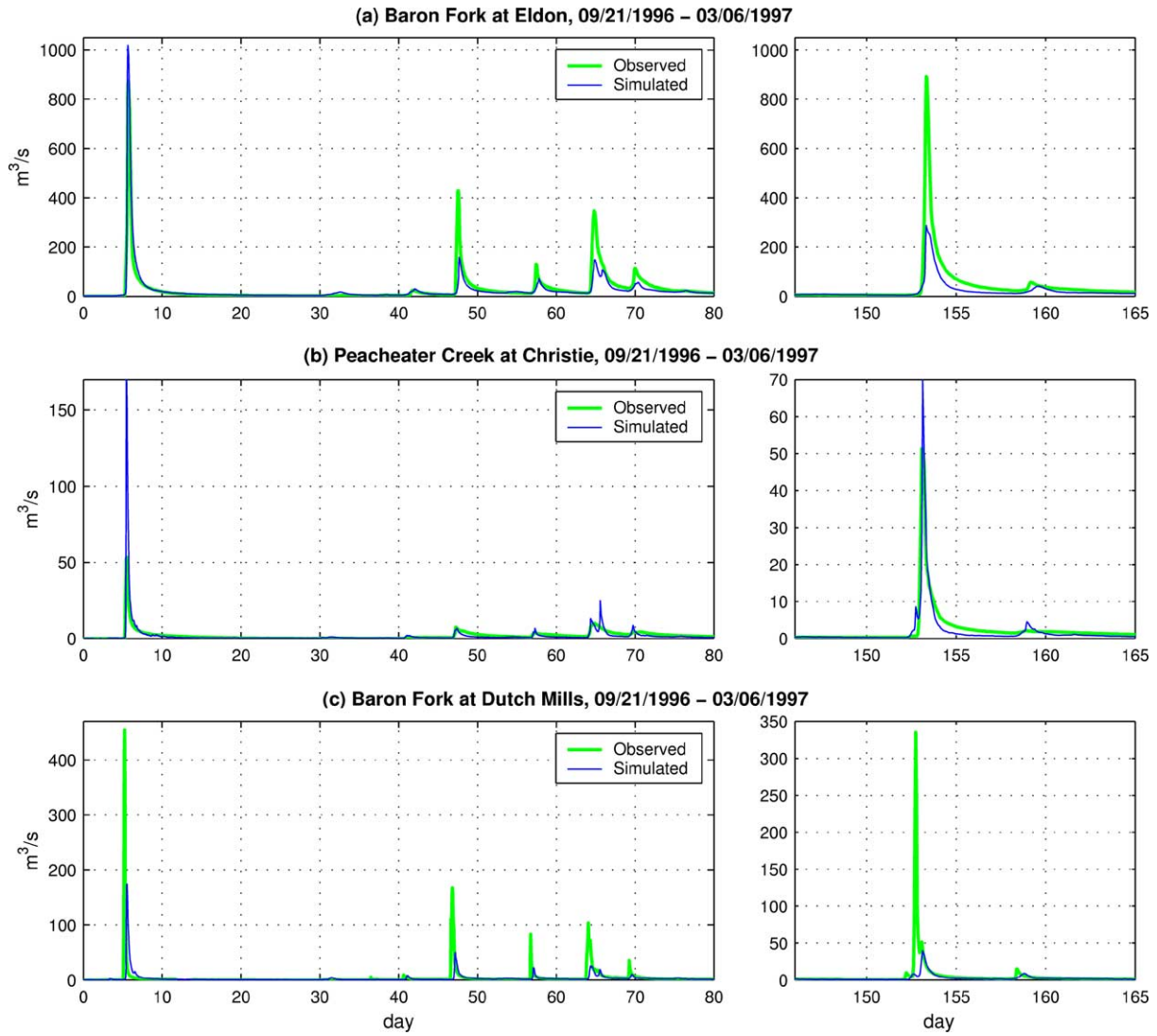

Fig. 3. An excerpt from a continuous run for Baron Fork illustrating simulation skills for the catchment outlet (a) and nested gaged locations: Peacheater Creek (b), and Baron Fork at Dutch Mills (c). The total period covers 5.5 months (09/21/1996–03/06/1997). The interstorm period, that occured between days 80 and 146, is not shown. The scale of *y*-axis on the right-side and left-side plots are different.

the simulated hydrologic variables, demonstrate how terrain, soils, and vegetation act in catchments having different land-surface properties. All of the presented results correspond to the simulations covering the entire DMIP period (the results were submitted in January 2003, for details see Reed et al., this issue).

5.1. Streamflow simulation

DMIP specified a calibration period between 06/1993 and 07/1999. Only limited manual calibration was performed for the Baron Fork and Blue River catchments for several events and interstorm periods of varying duration within the specified time interval. Calibrated parameters for the Baron Fork basin were directly transferred (without further calibration) to simulate the hydrologic regime of the Illinois River at Watts catchment. Continuous simulations spanning the period 06/1993–07/2000 were performed following the 4–7 month spin-up periods of the groundwater dynamics for each of the basins. This decreased the effect of local inconsistencies in the model initialization while attaining the observed baseflow rates prior to the beginning of the simulation period.

5.1.1. Overall statistics

The common measure of model performance is the comparison of the simulated and observed discharge hydrographs at the catchment outlet. A variety of statistics, in terms of flow volume, timing, and variability are used to evaluate streamflow modeling skills (see Appendix A). Table 3 (see Appendix A for definition of terms) presents multi-year statistics of

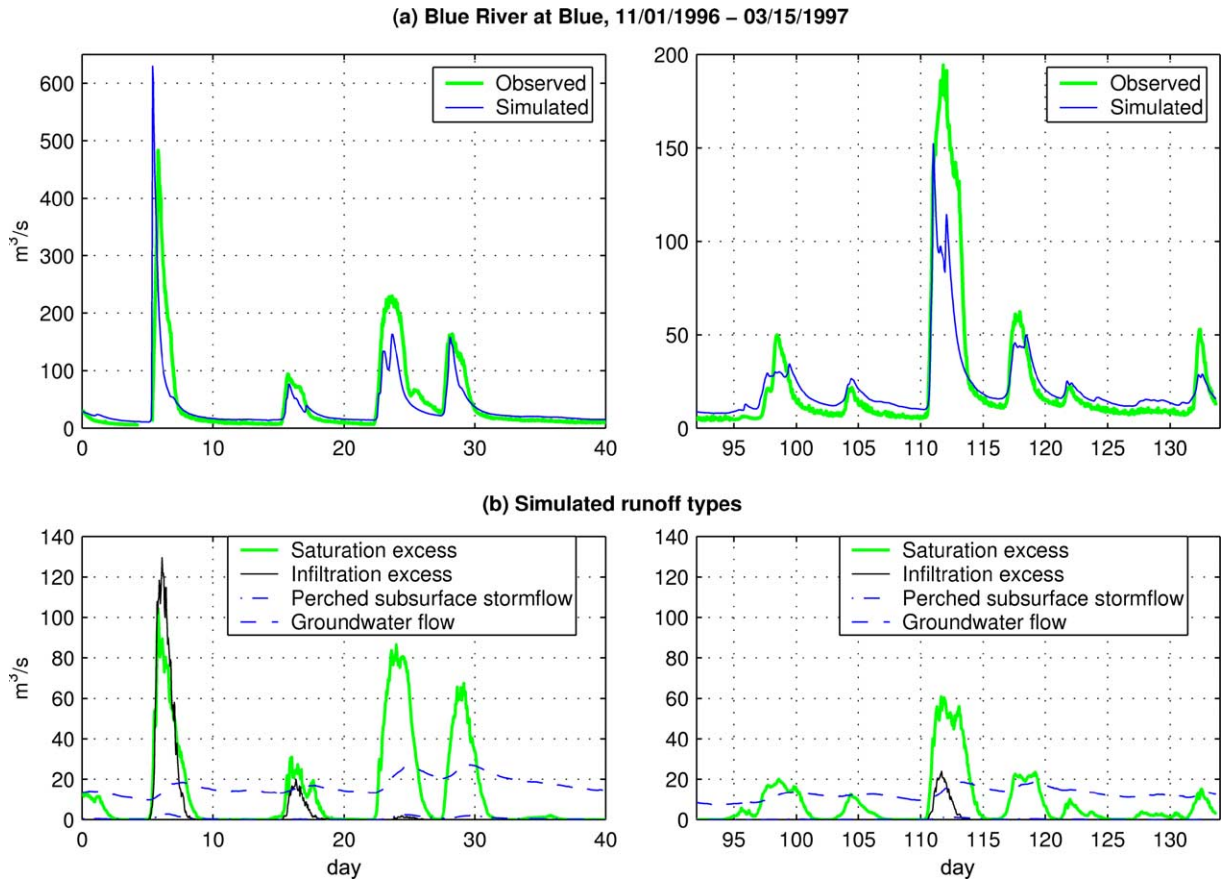

Fig. 4. An excerpt from a continuous run for Blue River illustrating simulation skills for the catchment outlet (a), and the approximate partitioning of the outlet streamflow into four runoff types (b). The total period covers 4.5 months (11/01/1996–03/15/1997). The interstorm period, that occured between days 40 and 92, is not shown. The scale of *y*-axis on the right-side and left-side plots are different.

the streamflow simulation for all gaged catchments. It can be concluded that the best performance was achieved for the Baron Fork basin. Interestingly, the results from the uncalibrated simulations for the Illinois River at Watts are also quite satisfactory, taking into account that parameter adjustments were not performed. Modelling results for the Blue River basin indicate that the model performance is best for the years 1997 and 1998 that include the events for which the model was calibrated. Model performance for the nested basins, e.g. Peacheater Creek and Illinois River at Savoy, is generally worse (Table 3) which can be partly attributed to the fact that streamflow data for these basins were neglected during calibration of the encompassing main basins.

5.1.2. Hydrographs

Selected excerpts from the continuous streamflow simulations for the outlet and nested locations are shown in Figs. 3–5. An example of how model performance can be affected by poor representation of the internal land-surface characteristics is given in Fig. 3. Streamflow series for the outlet point are given in the top plot, in which the first event, dominated by the infiltration excess runoff, was among those used to calibrate the model. While the difference between the observed and simulated series is minimal at the outlet point, the model either overestimates (Peacheater Creek) or underestimates (Baron Fork at Dutch Mills) runoff volume in the nested locations. Ignoring information at the internal points implies poor representation of the land-surface properties and results in systematic bias when internal compensation does not occur (later events shown in Fig. 3). Fig. 4 shows differences in basin response which are highly dependent on rainfall spatial location and magnitude. The bulk of the response to the first rainfall event is almost equally composed of infiltration excess

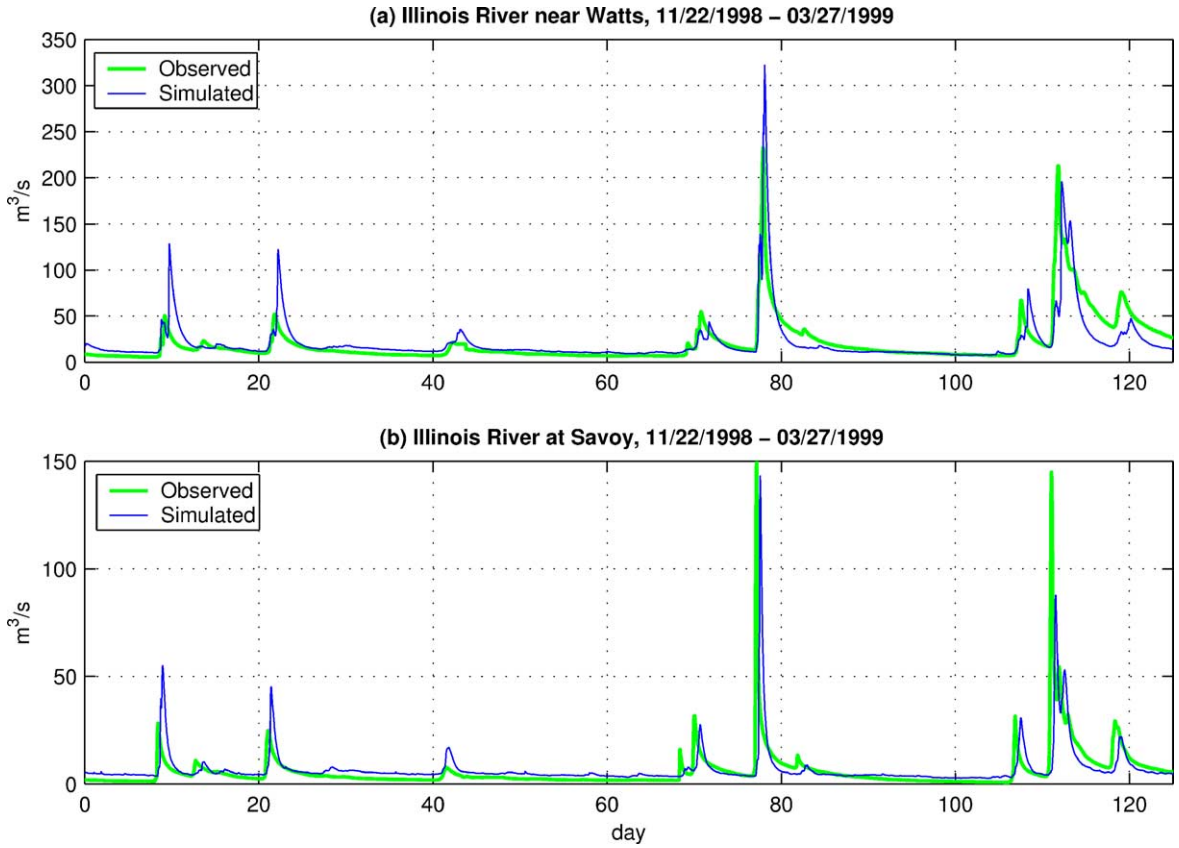

Fig. 5. An excerpt from a continuous run for Illinois River illustrating model performance for the catchment outlet (a), and a nested location — Illinois River at Savoy (b). The total period covers 4 months (11/22/1998–03/27/1999).

and saturation excess flow. The high magnitude and quick response indicate that most of the rainfall occurred in the catchment south-eastern region which is composed of primarily clayey soils (Fig. 2). The saturation excess mechanism dominates the hydrologic response in most of the subsequent events. An excerpt from a continuous simulation for Illinois River is shown in Fig. 5. As it can be seen, the model performance is quite satisfactory considering the fact that the simulation used parameters transferred from the calibration for a neighboring basin (Baron Fork).

5.1.3. Seasonal flows

Results obtained with physically-based approaches can be used to determine which process representations can be improved by either adjusting the model parameters, data, or introducing a more efficient process parameterization. In this context, spatially lumped quantities, such as streamflow, can be disaggregated to represent the components that reveal different underlying physical mechanisms. Fig. 6 shows the composition by runoff type of the mean simulated monthly flow as well as the mean observed

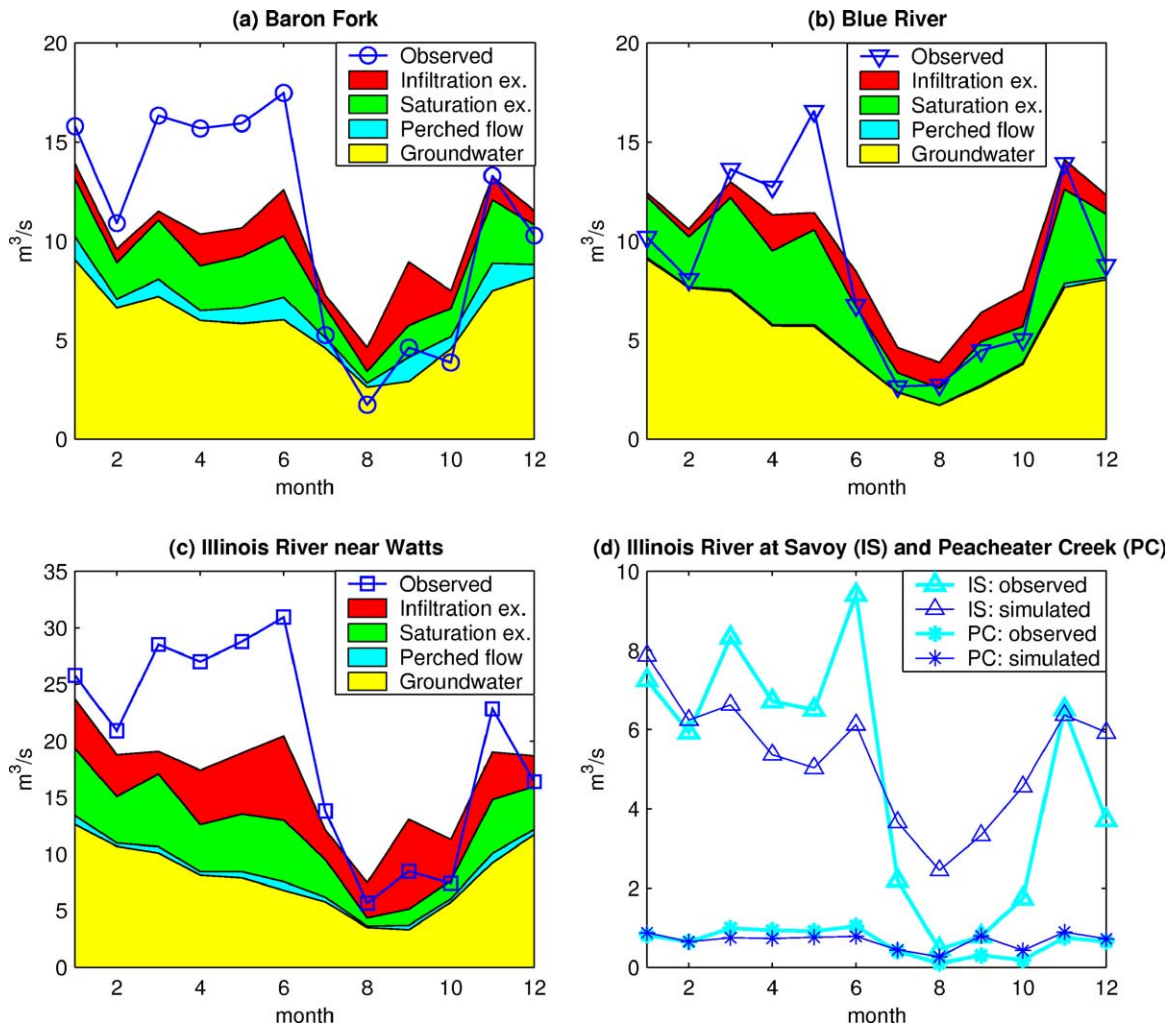

Fig. 6. Partitioning of the simulated monthly streamflow into runoff types and the mean observed monthly streamflow for the major test basins: (a) Baron Fork at Eldon, (b) Blue River at Blue, and (c) Illinois River at Watts. Only the mean simulated and observed monthly streamflow are illustrated for the two nested gaged locations (d) Illinois River at Savoy and Peacheater Creek at Christie. The total analysis period covers 04/01/1994–07/31/2000.

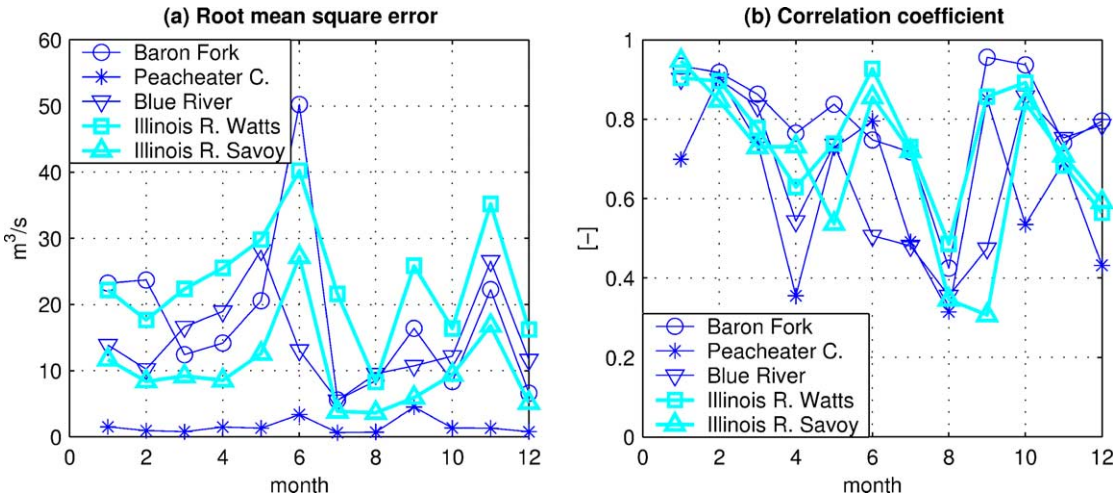

Fig. 7. Monthly root mean square error (a) and correlation coefficient (b) of the simulated streamflow series with respect to the observed series for the test basins. The total analysis period covers 04/01/1994–07/31/2000.

flows; while Fig. 7 shows the corresponding monthly errors and correlations. As it can be seen in the figures, the model consistently underestimates spring flows (months 3–6) resulting in large root mean square (RMS) errors. A plausible explanation is that the dynamics of the saturated zone are not correctly accounted for during the spring period, which is generally wetter than the rest of the year. A higher relative proportion of groundwater and saturation excess flow should be expected. Such inadequacy of the simulation results can be a consequence of both the model physics (incorrect dynamics of lateral moisture redistribution) and insufficient knowledge about land-surface properties, for example, bedrock depth. Overestimation of low-flows during the summer periods results in lower correlation coefficients with small RMS errors. To some extent, such a result can be related to the model performance during spring months: some of the 'spring' groundwater is actually produced 2–3 months later. For instance, as it can be seen in Fig. 5, the recession limb of the two last simulated events (in February and March of 1999) drops too fast, implying too quick of a depletion of water from the saturated zone. At the same time, during summers (months 6–9), the simulation results show that, in particular for Baron Fork and Illinois River, the simulated baseflow rates are usually higher than the observed. One also notices that for Illinois River at Watts (Fig. 6(c)) there is an obvious overestimation problem with the infiltration excess runoff type that is equal to about 100% of the observed monthly flow in September.

5.1.4. Cumulative flows

Cumulative flow over the simulation period indicates consistency of the model performance skills. It may also point to the deficiencies of simulation. Such periodic increases and decreases superimposed upon the general increase in difference between the observed and simulated cumulative flows for Baron Fork and Illinois River near Watts catchments (Fig. 8(a) and (c)) can be attributed to the previously mentioned underestimation of spring flows and overestimation of the summer discharges. Simulated cumulative flows for the nested basins, Peacheater Creek and Illinois River at Savoy, tend to exceed the observed flows, because overestimated summer streamflows exceed underestimated spring discharges. The same pattern can be observed for the Blue River basin. A sudden change towards a positive difference at month 55 (Fig. 8(b)), 10–11/1998, however, may indicate a change in the data quality for this basin (streamflow or input hydrometeorological forcing). Results obtained with other models show the same tendency (Reed et al., this issue).

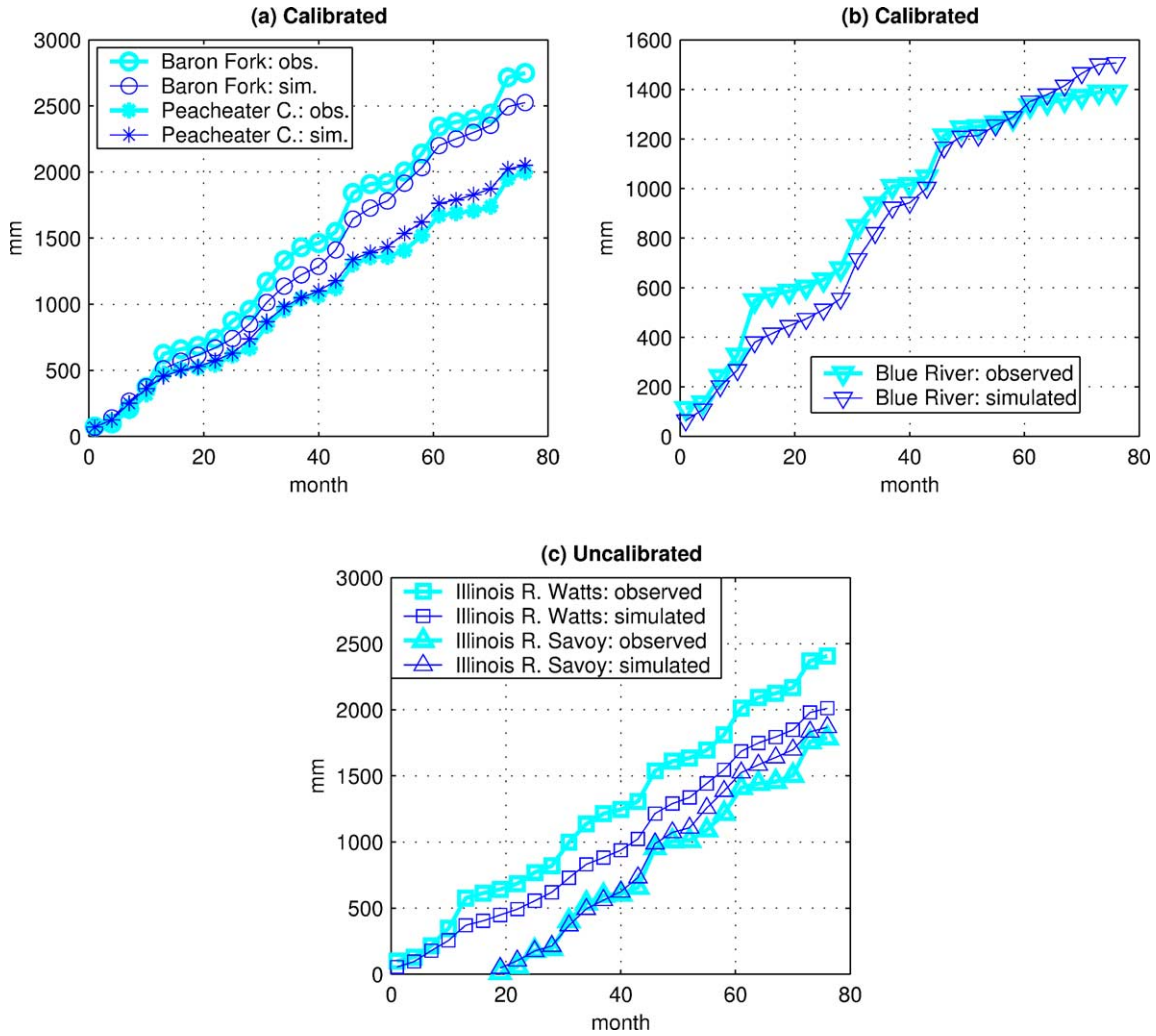

Fig. 8. Accumulated observed and simulated streamflow for calibrated ((a) and (b)) and uncalibrated basins (c). The total analysis period covers 04/01/1994–07/31/2000.

5.2. Spatial simulation of rainfall–runoff process

Spatial fields of state variables exhibit patterns that represent variability of hydrologic response due to the combined effects of rainfall, topography, soils, and landuse/vegetation. Fig. 9 shows spatial fields at 12 p.m. on January 5th 1998, of several state variables simulated during a continuous run for the Blue River basin. As a consequence of a rainfall event that started 44 h earlier, instantaneous runoff production (a), rate of lateral exchange in the unsaturated zone (b), soil moisture in the top 10 cm of soil (c), and water table depth (d) showed significant spatial variability. One notices the pronounced effects of topography and soils on the basin state.

The first moments of the state variables provide site specific characteristic properties of the hydrological dynamics. For instance, Fig. 10 shows mean soil water content in the top 1 m of soil evaluated over a simulation period of 06/1993–07/2000. This state variable, used as a surrogate for the soil moisture content in the root zone, displays significant dependence on the soil texture and topography. For instance, clayey soils, having large water retaining

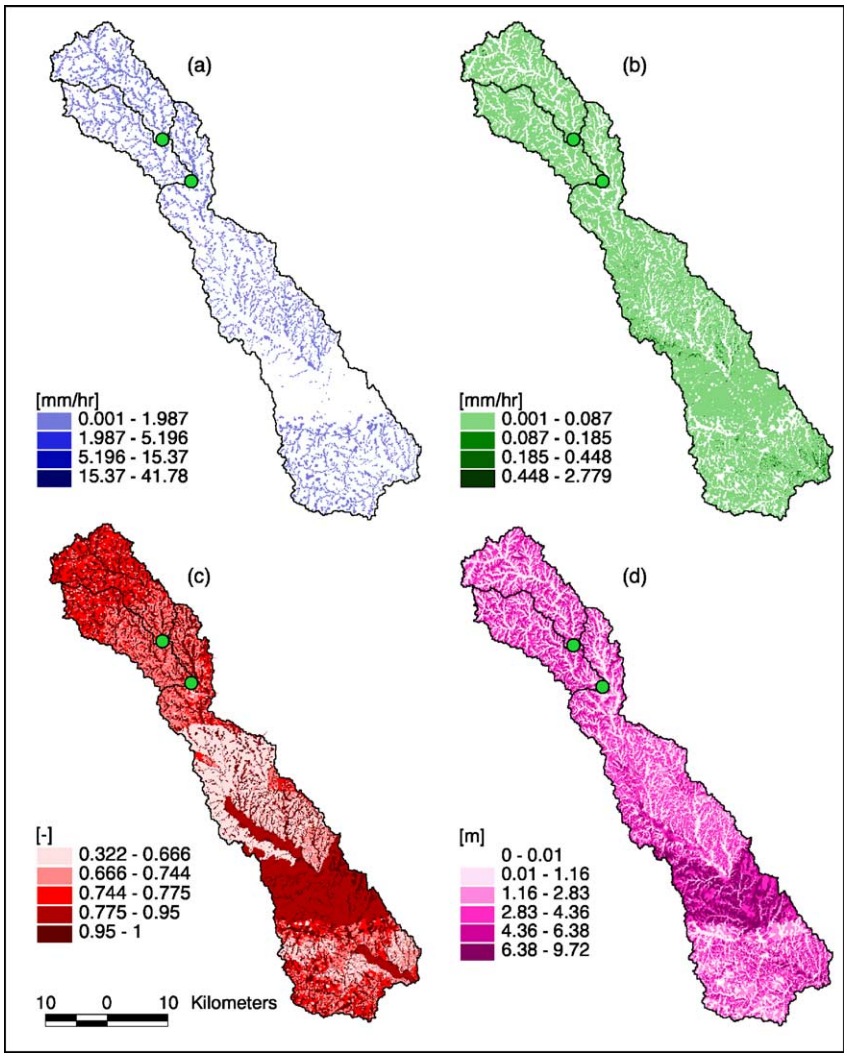

Fig. 9. State variables simulated during continuous run at 12 p.m. on January 5th 1998, for the Blue River basin: (a) instantaneous runoff production, (b) rate of lateral exchange in the unsaturated zone, (c) soil moisture in the top soil 10 cm, (d) water table depth.

properties, show higher average moisture contents, while sandy soils exhibit lower values of the mean soil water content due to intrinsically higher drainage characteristics (Figs. 2 and 10). Convergent terrain areas show consistently larger values of the moisture content although one notices that topography has diverse effects on soils having different texture type (e.g. clays as opposed to loams).

Evaporative fraction, defined as the ratio between latent heat flux and available energy, is a representative indicator of the relative wetness conditions of a site since evaporation explicitly depends on the amount of moisture contained in the upper soil layer. Mean values of evaporative fraction simulated for the Baron Fork basin over the same period as above (06/1993–07/2000) are shown in Fig. 11. Variability across the terrain can be clearly discerned: higher values are attributed to convergent hillslope bottom areas as well as to the flat areas in the basin headwaters (north-east corner in the bottom left plot

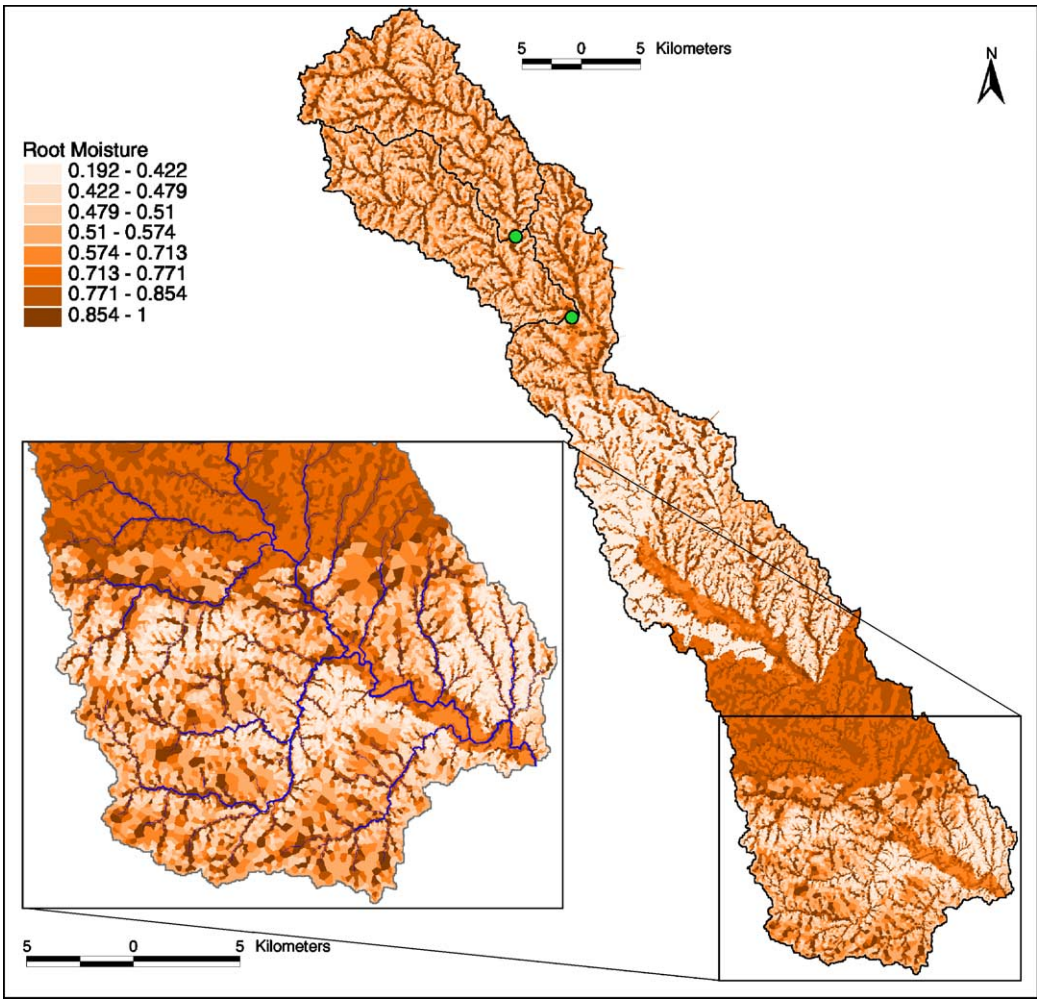

Fig. 10. Mean soil moisture content in the top 1 m of soil evaluated over a simulation period of 06/1993–07/2000 for the Blue River basin.

of Fig. 11) where lateral redistribution fluxes are negligible. Steep slopes show lower values of evaporative fraction as a result of higher drainage of moisture from the vadose zone in the form of interflow. One may also notice that there is a substantial difference between grassy and forested sites, the latter being more conductive and having higher soil conductivity anisotropy. Sloped forested sites are thus more efficient in lateral moisture redistribution leading to less residence times of infiltrated water in the unsaturated zone and faster convergence of subsurface fluxes at the hillslope bottom.

Fig. 12 shows the spatial distribution of relative frequencies of saturation excess runoff as a percentage of the total run time over 7 years of simulation for the Blue River basin. Locations of the most frequent occurrence of saturation excess runoff reflect the perennial stream network of the catchment. Locations of lower frequency of runoff occurrence are attributed to sites of lower topographic index, midline, and groundwater recharge regions (see Section 5.3). Soil texture type also significantly affects the magnitude and variability of saturation runoff occurrence across the catchment terrain. As one can see in Fig. 12, this runoff type occurs in clayey soils quite rarely. The reason for that are both low infiltration capacity and low lateral rates of moisture redistribution that are typical for clay soils.

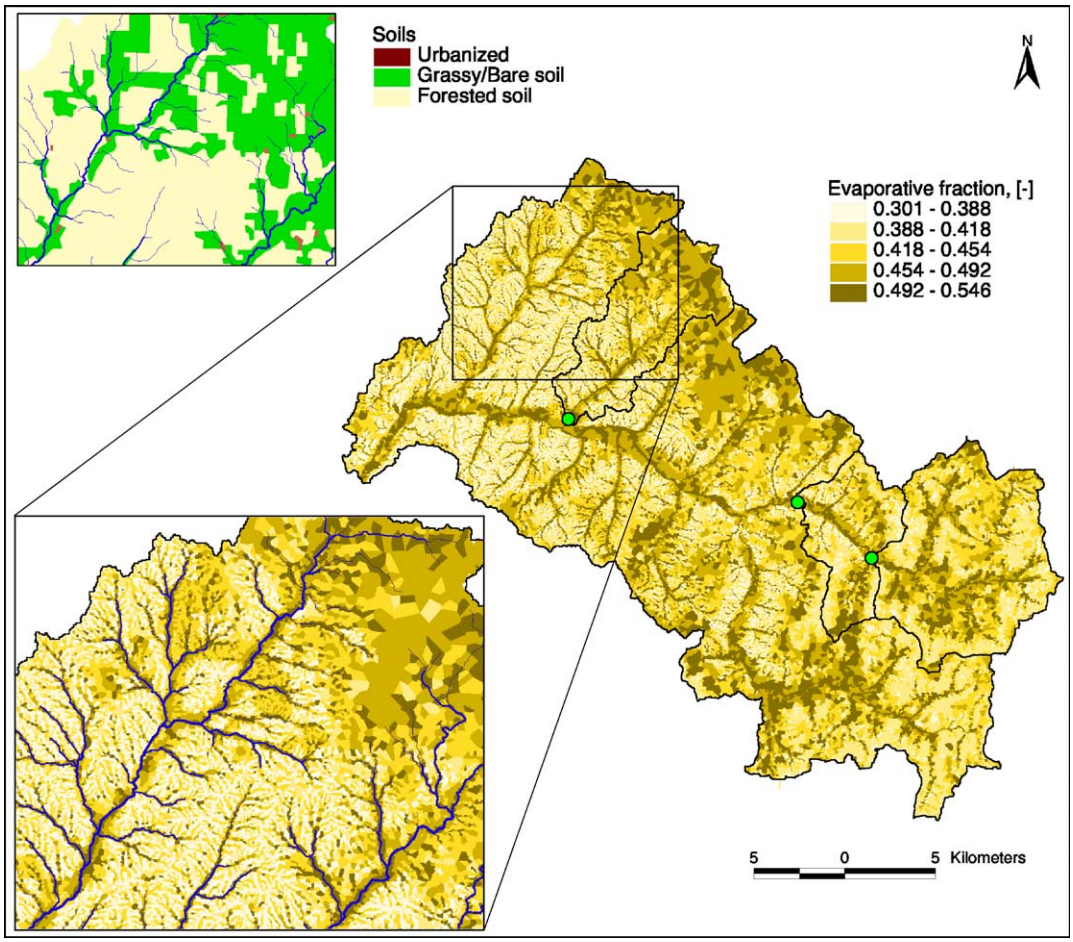

Fig. 11. Mean evaporative fraction evaluated over a simulation period of 06/1993–07/2000 for the Baron Fork basin.

5.3. Land-surface controls on catchment hydrologic regime

5.3.1. Controls due to land-surface features

Topography and soil controls on hydrologic regime, presented in the combined form of spatial coverages in Figs. 10–12, can be shown via relationships that single out the integral effect of each factor. For example, Fig. 13 shows the mean root zone soil moisture as a function of the topographic index for different soil types (illustrated previously in Fig. 10). Vertical bars from points in the plot represent standard deviations of the values computed for the corresponding bins. As Fig. 10 shows, there is a strong dependence of the mean soil moisture value on the topographic attributes of a site. Variability of the soil water content, i.e. magnitude of the standard deviation within a bin, is also related to the terrain location and is relatively smaller or larger for certain ranges of the topographic index (more pronounced in the case of Blue River basin). It is suggested that such differences in the magnitude of soil moisture variability can be attributed to the differences in the degree of coupling between the processes induced at the land-surface and subsurface lateral moisture exchange. For instance, small variability of the root zone soil moisture for topographic indices less than 10–12 in Fig. 13(a) and (b) can be associated with the sites where the processes of infiltration and evapotranspiration are not affected by the groundwater dynamics

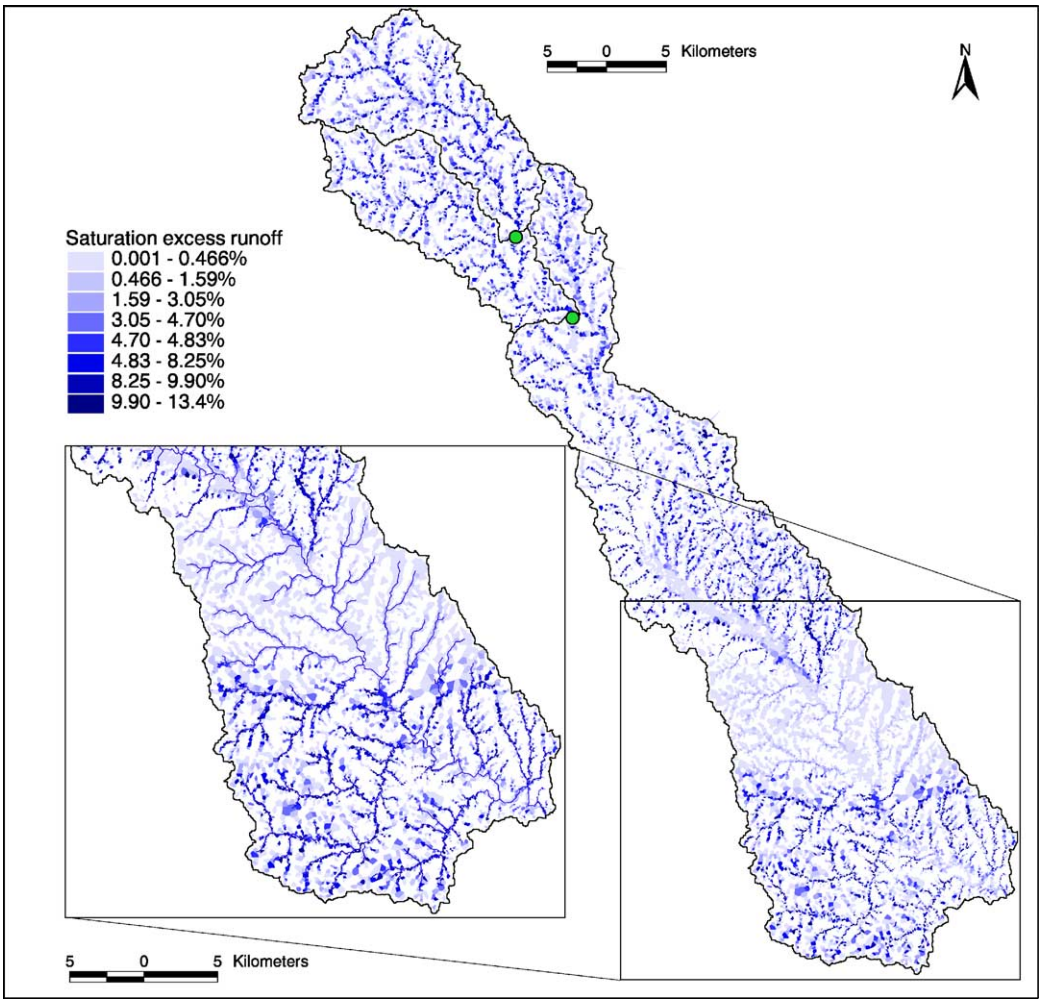

Fig. 12. Frequency of occurrence of saturation excess runoff as a percentage of the total simulation period (06/1993–07/2000) for the Blue River basin.

and the lateral redistribution of water in the vadose zone is insignificant. The total soil moisture variability at a site can thus be explained for the most part by the contributions from rainfall variability and variability of potential evapotranspiration demand, both are climatically dictated. Higher variability of the soil water content in the range of topographic indices 13–25 (Fig. 13(b)) can likely be attributed to the periodic wetting and drying of the groundwater as well to the transient dynamics of fluxes in the unsaturated zone that exhibit strongly non-linear dependence on storm magnitude and soil texture type. Decrease of soil moisture variability at higher values of the topographic index is presumably due to a more permanent contribution from the groundwater. As it can be seen, soil texture has a significant impact on magnitude and variability of the root zone soil moisture. For example, the three soil types chosen for the Blue River basin: loamy fine sand, loam, and clay, show significantly different magnitudes and variability of the mean soil moisture content (Fig. 13(b)).

Topography also affects moisture dynamics through its impact on the local energy balance. Fig. 14 shows the relationship between mean

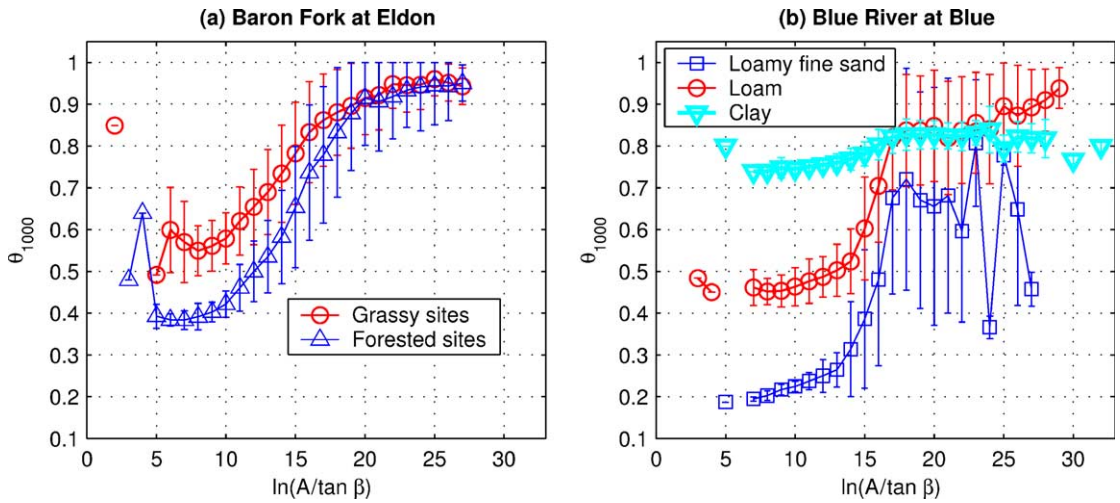

Fig. 13. Mean soil moisture content in the top 1 m of soil (surrogate value for a root zone), θ_{1000}, in relation to the topographic index, $\ln(A/\tan\beta)$, for (a) Baron Fork and (b) Blue River basins. A is the surface contributing area (km^2), β is the land-surface slope angle of an element.

evaporative fraction and aspect of an element. Aspect is measured as the clock-wise angle (in radians) between the northern and flow direction of the element. For example, a value of 3.14 implies element facing south, and a slight increase in the evaporative fraction at this value can be attributed to larger amount of incoming short wave solar radiation. The relationship between the mean evaporative fraction and the mean root zone soil water content are shown in Fig. 15 separately for each soil type. Although the functions that constrain evapotranspiration from the potential rate depending on the soil moisture availability in the upper soil layer are linear (Ivanov et al., 2004), the resulting time-integrated relationship exhibits non-linearity for all soil types.

Topography and soil controls on runoff generation mechanisms are shown in Figs. 16 and 17 for the Baron Fork and Blue River basins correspondingly.

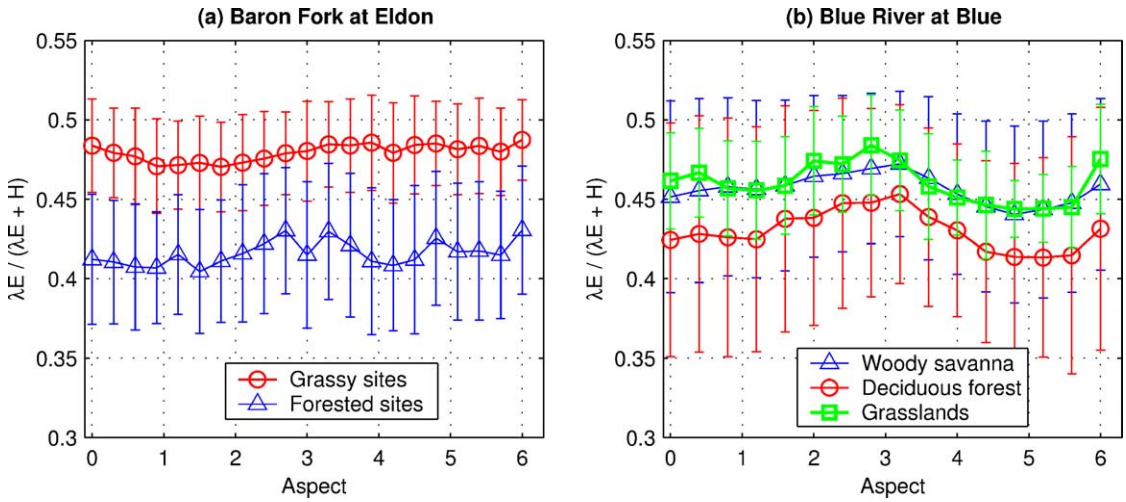

Fig. 14. Evaporative fraction, $\lambda E/(\lambda E + H)$, in relation to the aspect of the element for (a) Baron Fork and (b) Blue River basins. λE is the latent heat flux, H is the sensible heat flux.

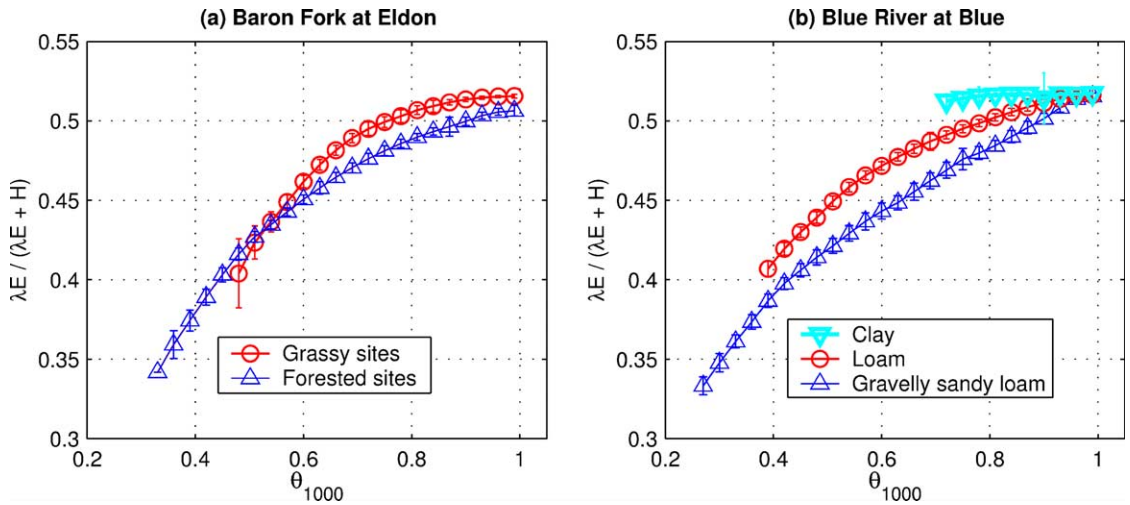

Fig. 15. Evaporative fraction, $\lambda E/(\lambda E + H)$, in relation to the root zone soil moisture, θ_{1000}, for (a) Baron Fork and (b) Blue River basins.

Relative frequencies of runoff type occurrence as a percentage of the total run time over 7 years of simulation for both basins are presented. Two common features can be discerned in Figs. 16 and 17. While occurrence of infiltration excess runoff is modulated both by soil texture type and topography, terrain features are for the most the essential factor regulating other runoff generation mechanisms: saturation excess, perched return flow, and groundwater flow. In the context of tRIBS, infiltration excess is caused by water accumulation in the unsaturated zone in conditions of low vertical and lateral redistribution rates (Ivanov et al., 2004). Within the model, runoff is considered to be of infiltration excess type when the redistribution rate of the top saturated layer is lower than the rainfall intensity, irrespective of the preceding infiltration history. Therefore, the occurrence of this runoff type explicitly depends on soil hydraulic properties by means of infiltration rates, as well as position of the site within the catchment terrain, via the intensity of subsurface moisture exchange. The maximum of occurrence of the infiltration excess runoff corresponds to values 12–14 of the topographic index (Figs. 16 and 17(a)) at which variability of the mean moisture content significantly increases (Fig. 13). It also corresponds to values of the topographic index at which occurrence of saturation excess and groundwater runoff types becomes increasingly non-negligible (Figs. 16 and 17(b–d)). The latter two types are produced only in cells where full saturation of the soil column is reached. In conjunction with the previous discussion, terrain locations that have topographic indices in the range of 12–14 may represent the boundary of the transitional zone between regions in which either the unsaturated or groundwater processes dominate overall hydrological dynamics. In these terrain locations, subsurface lateral exchange in the vadose zone leads to the highest accumulation of moisture at the top of the unsaturated zone and the effect of groundwater on surface processes becomes increasingly significant.

Fig. 18 shows average rates of infiltration excess runoff generated in different soils for the same basins. More clayey, less conductive soils, which produce this runoff type more frequently (Figs. 16 and 17), exhibit a quite uniform distribution of rates over the entire range of topographic indices (Fig. 18(a) and (b)). More frequent rainfall events of lower intensity ($<$7–10 mm/h), which contribute largely to the mean rate value, are sufficient to produce infiltration excess runoff in these soils. For more conductive soils (forested, for the case (a), or sandy loam for the case (b), Fig. 18), rainfall of extreme intensities and substantial accumulation of moisture due to lateral exchange in the unsaturated zone are necessary to result in production of infiltration excess runoff. Terrain locations of maximum runoff rates in these soils correspond to

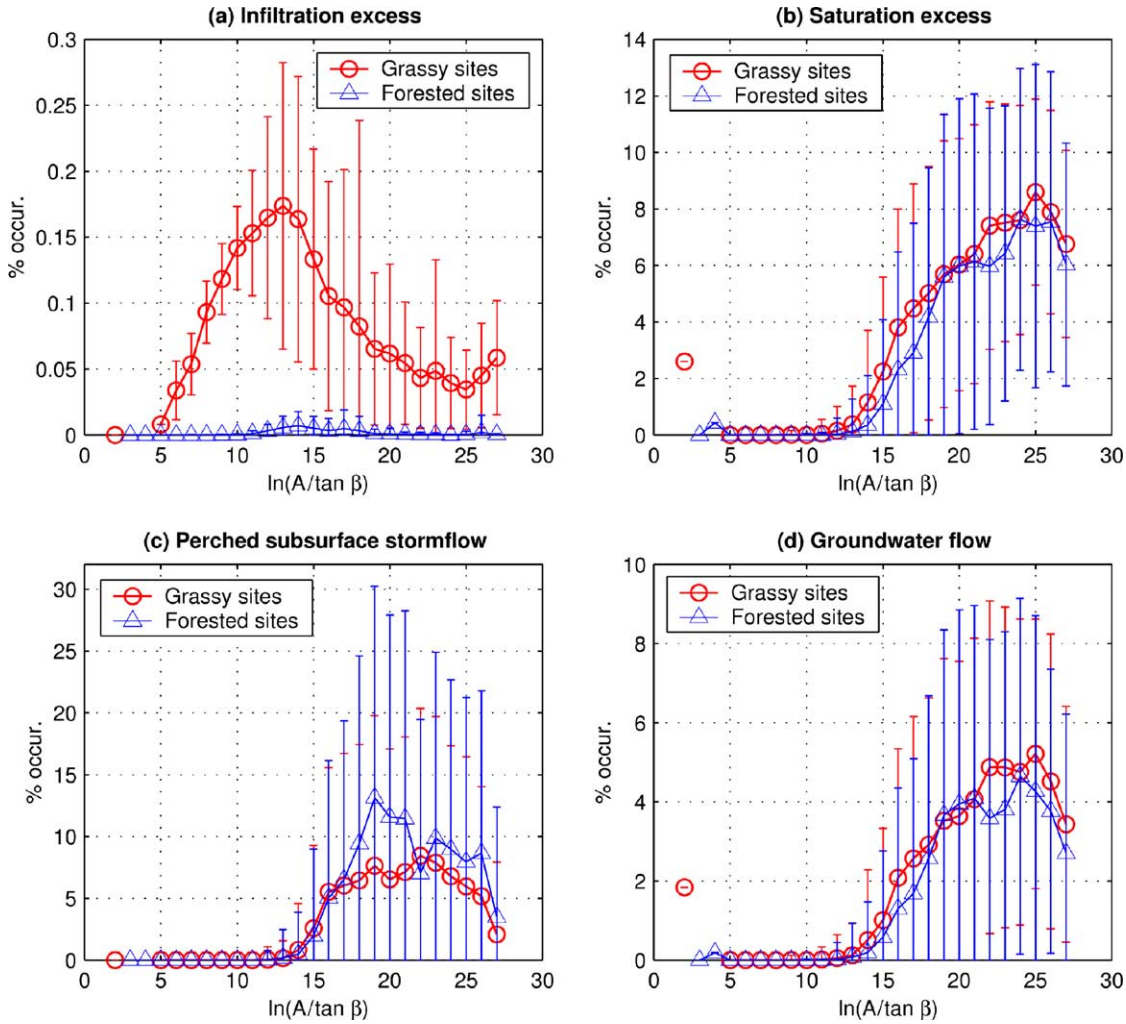

Fig. 16. Frequency of occurrence of runoff production events as percentage of the total simulation period 06/1993–07/2000 for different soil types in relation to the topographic index, $\ln(A/\tan\beta)$, for the Baron Fork basin: (a) infiltration excess, (b) saturation excess, (c) perched subsurface stormflow, (d) groundwater flow.

the areas where moisture accumulation is the highest. As seen from Fig. 18, the maximum rates correspond to the range of the topographic indices between 12 and 15.

5.3.2. Controls due to subsurface dynamics

The long-term net flux across the water table can be used to discern regions where the net exchange in the saturated zone tends to be positive, negative, or deviating around zero. The hillslope areas can be correspondingly classified into groundwater recharge, discharge, or midline regions (Freeze and Cherry, 1979; Salvucci and Entekhabi, 1995; Levine and Salvucci, 1999). In the following examples, partitioning of elements into these characteristic regions was performed by analyzing the net water table change and runoff production by saturation excess and groundwater mechanisms. Since this classification is based on the local groundwater dynamics, it allows for qualitative discrimination between regions where the groundwater dominates overall dynamics and regions where

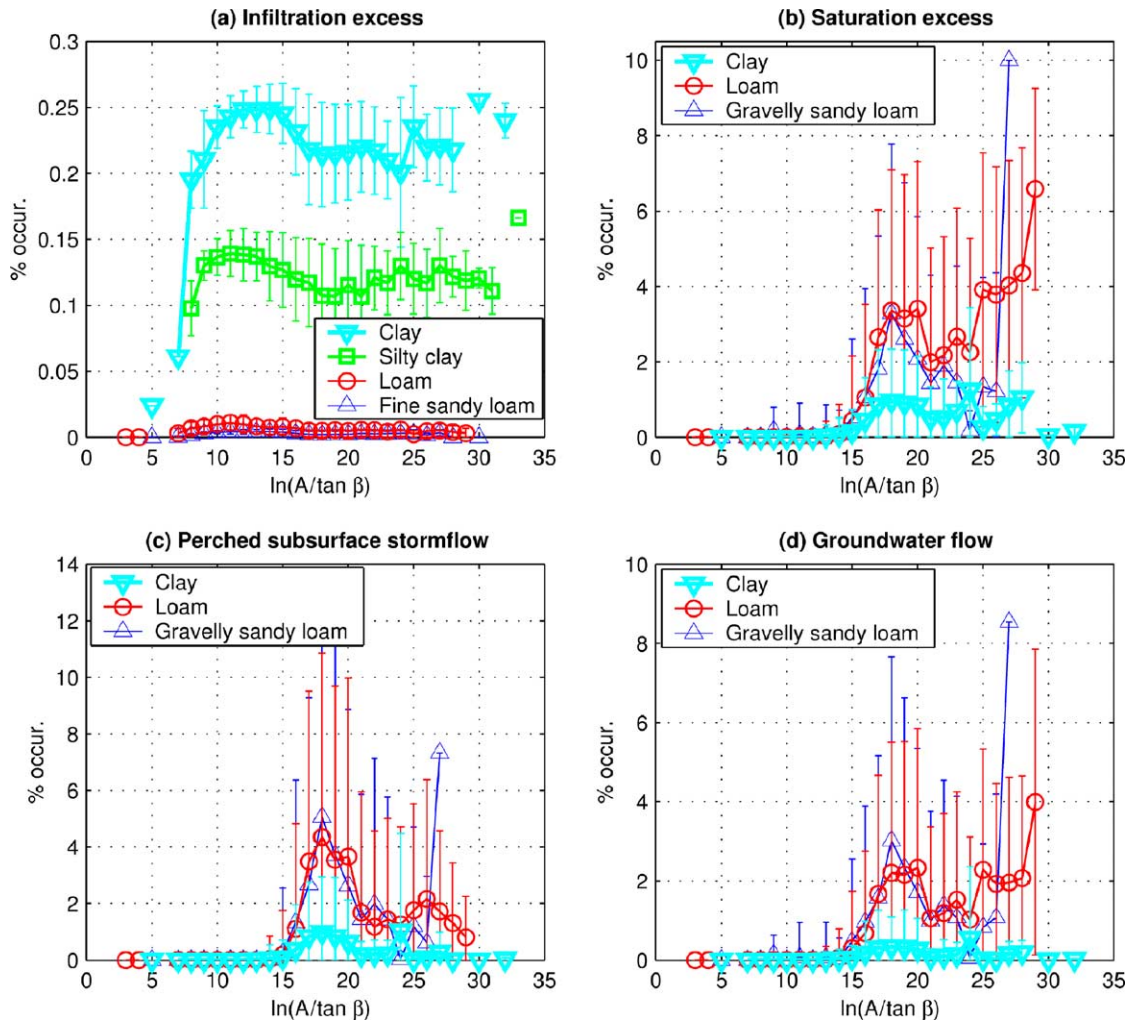

Fig. 17. Frequency of occurrence of runoff production events as percentage of the total simulation period 06/1993–07/2000 for different soil types in relation to the topographic index, $\ln(A/\tan\beta)$, for the Blue River basin: (a) infiltration excess, (b) saturation excess, (c) perched subsurface stormflow, (d) groundwater flow.

its effects are periodic or negligible. It is therefore worthwhile to analyze hydrological variables in these regions and their relation to the topography.

Figs. 19 and 20 present the root zone soil moisture related to the topographic index of a site for each characteristic groundwater dynamics region within a particular soil type. Both for the Baron Fork and Blue River basins, groundwater discharge regions show substantially higher mean moisture values over the upper range of values of the topographic index. One may also notice that for less conductive soils, such as grassy sites in the Baron Fork basin or clay and loam soils in the Blue River basin, discharge regions are attributed only to the topographic locations beyond certain threshold value, 10–11 for both basins. For more conductive soils (forested—for the Baron Fork basin or loamy fine sand and fine sandy loam soils for the Blue River basin) magnitude and variability of the root zone soil moisture of the discharge and midline region exhibit a sharp increase in the range of topographic indices at values between 12 and 15. This is consistent with the previous discussion.

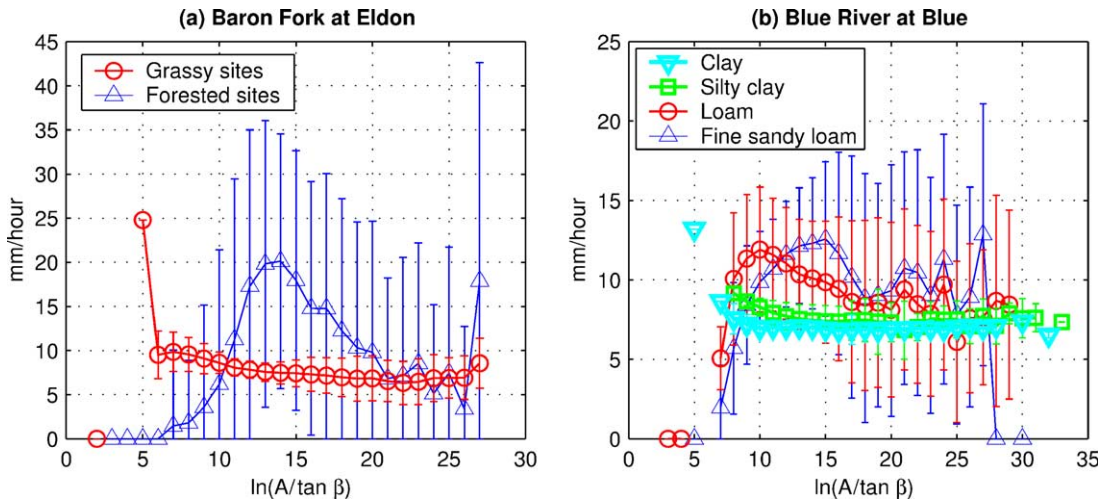

Fig. 18. Mean rates of infiltration excess runoff evaluated over the total simulation period 06/1993–07/2000 in relation to the topographic index, $\ln(A/\tan\beta)$, for (a) Baron Fork, (b) Blue River basins.

Figs. 21 and 22 show the relationship between the groundwater dynamics and runoff generation mechanisms for the Baron Fork and Blue River basins. Infiltration excess runoff does not have any clear relation to any of the regions for the Baron Fork basin. For the Blue River catchment, this runoff type is attributed to the recharge region but, in essence, this happens due to the fact that the recharge region is 88% composed of clay and silty clay soils. As expected, the three runoff generation mechanisms that can occur only in completely saturated soils: saturation excess, perched subsurface stormflow, and groundwater flow, are all attributed to the groundwater discharge regions.

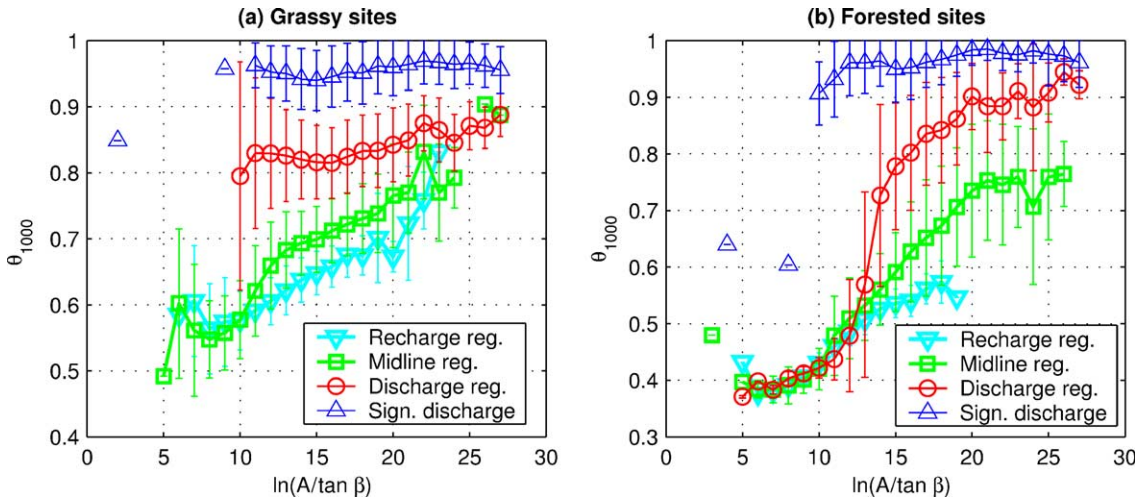

Fig. 19. Mean root zone soil moisture content, θ_{1000}, in relation to the topographic index, $\ln(A/\tan\beta)$, for different groundwater dynamics regions and soil types for the Baron Fork basin: (a) grassy sites, (b) forested sites.

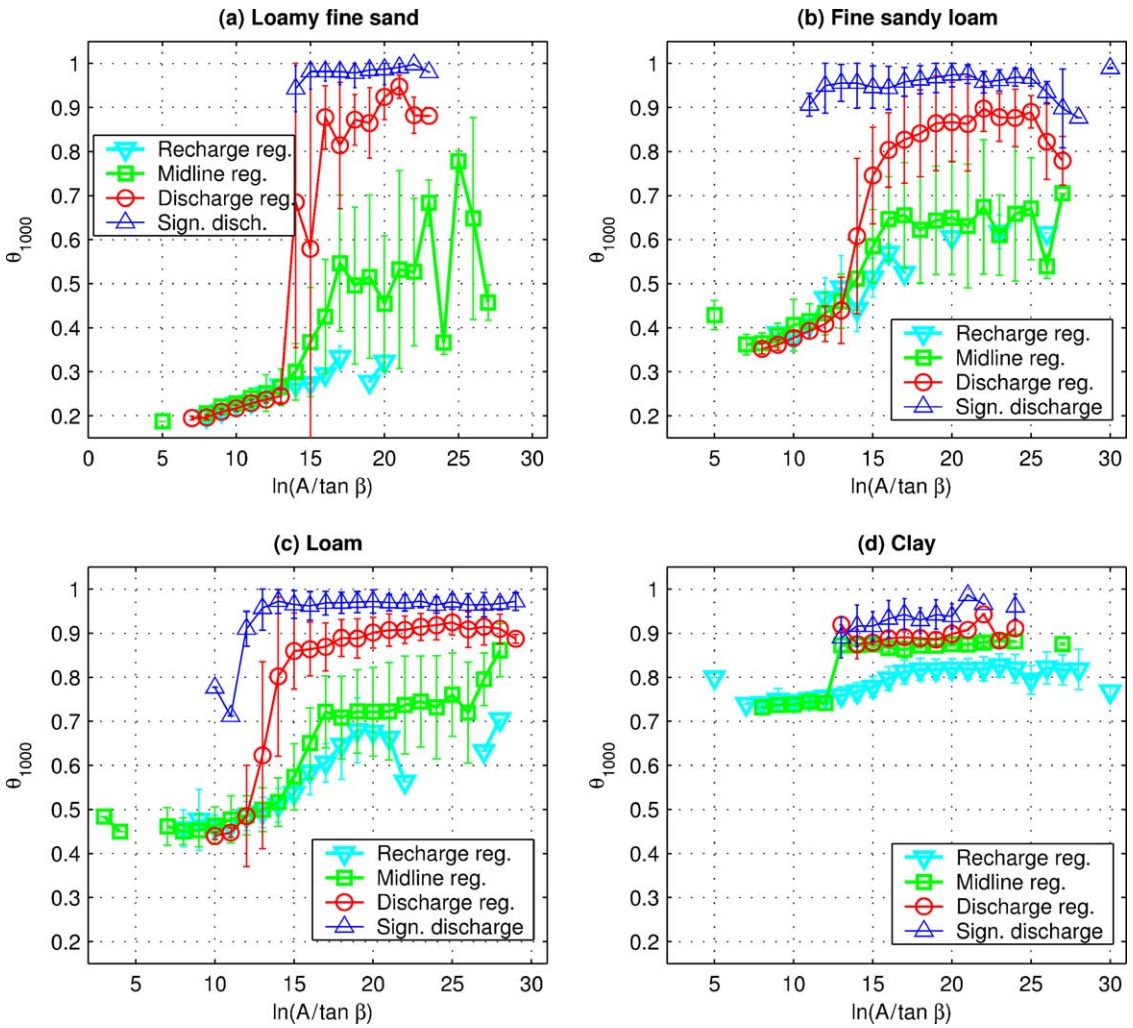

Fig. 20. Mean root zone soil moisture content, θ_{1000}, for different groundwater dynamics regions and soil types in relation to the topographic index, $\ln(A/\tan\beta)$, for the Blue River basin: (a) loamy fine sand, (b) fine sandy loam, (c) loam, (d) clay.

6. Conclusions

This paper presents the results of application of the fully-distributed, physically-based hydrological model tRIBS to a number of operational watersheds in Oklahoma and Arkansas within the framework of the Distributed Model Intercomparison Project (DMIP). The continuous hydrologic simulation for the total period of 7 years was feasible because of the use of irregular spatial resolution in representing the study catchments. While only limited manual streamflow-based calibration was performed, the results are promising. Various aspects of model simulation have been illustrated: streamflow at the outlet and interior locations, spatial fields of instantaneous and time-integrated hydrological variables, and relationships between land-surface descriptors and the key state variables. The value of distributed information in terms of discharge, topography, and soils has been demonstrated.

The paper attempts to address the potential for utilizing fully-distributed approaches at the scales of operational hydrologic forecasting. While catchment

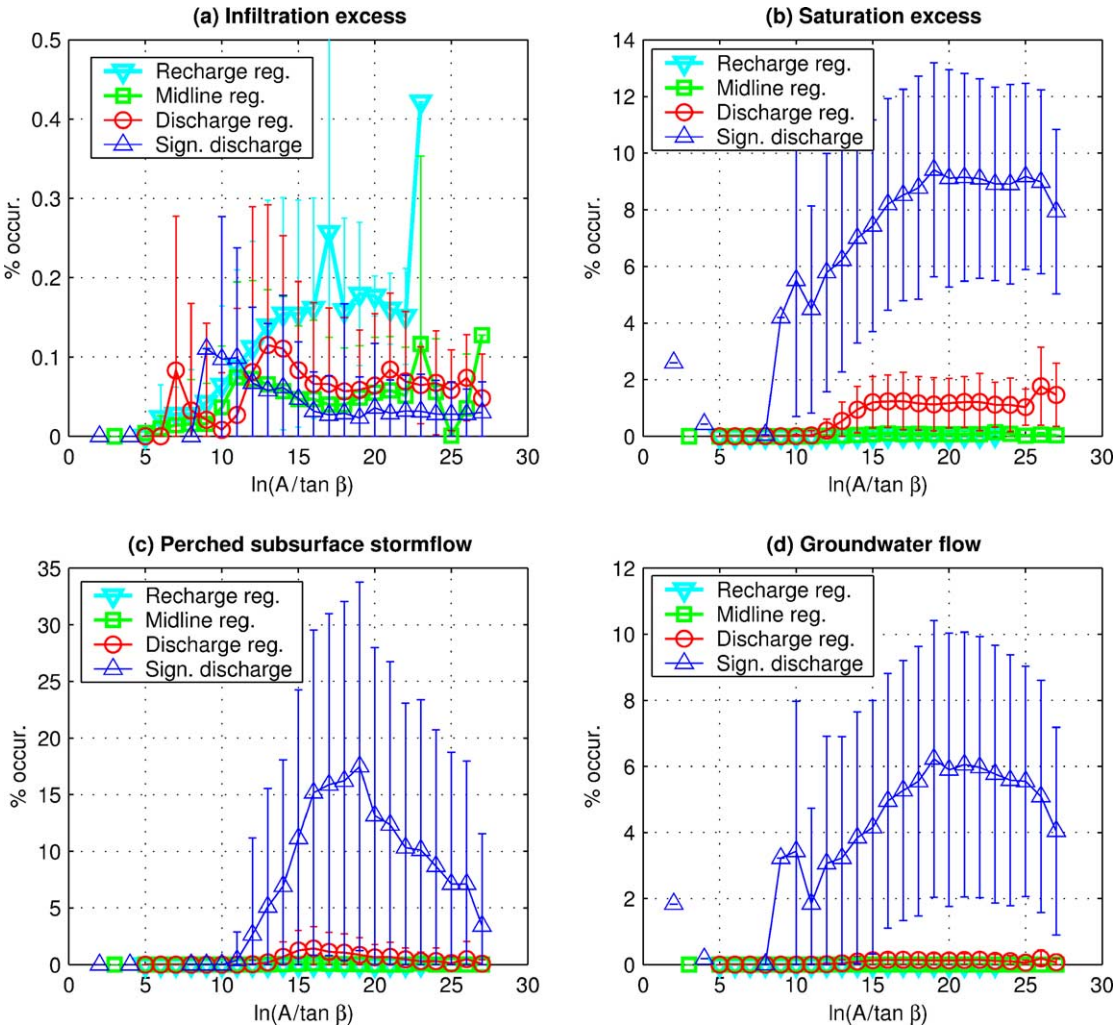

Fig. 21. Frequency of occurrence of runoff production events as percentage of the total simulation period 06/1993–07/2000 for different groundwater dynamics regions in relation to the topographic inde, ln(A/tan β), for the Baron Fork basin: (a) infiltration excess, (b) saturation excess, (c) perched subsurface stormflow, (d) groundwater flow.

outlet hydrographs were the only used measure for testing reliability of the model simulations, the presented results address a variety of aspects that concern spatial modeling capabilities. The essential strength of spatially-explicit methodologies is both in accounting for the time-invariant land-surface properties (e.g. topography) and predicting continuous fields (e.g. soil moisture) and point variables (e.g. streamflow) of state variables that are amenable for integration with observable physical quantities. Through a synthesis, between, for example, remote sensing data (e.g. McLaughlin, 1995; Reichle et al., 2001) and hydrologic modeling, the true value of the distributed approach should be realized, notwithstanding the difficulties that are associated with model parameterization and calibration. The breakthrough in accepting distributed approaches as the conventional tool of assessment will come, perhaps, from earth-science applications where the capability to generate spatially-distributed physical predictors and states will be as crucial as the capability to simulate streamflow.

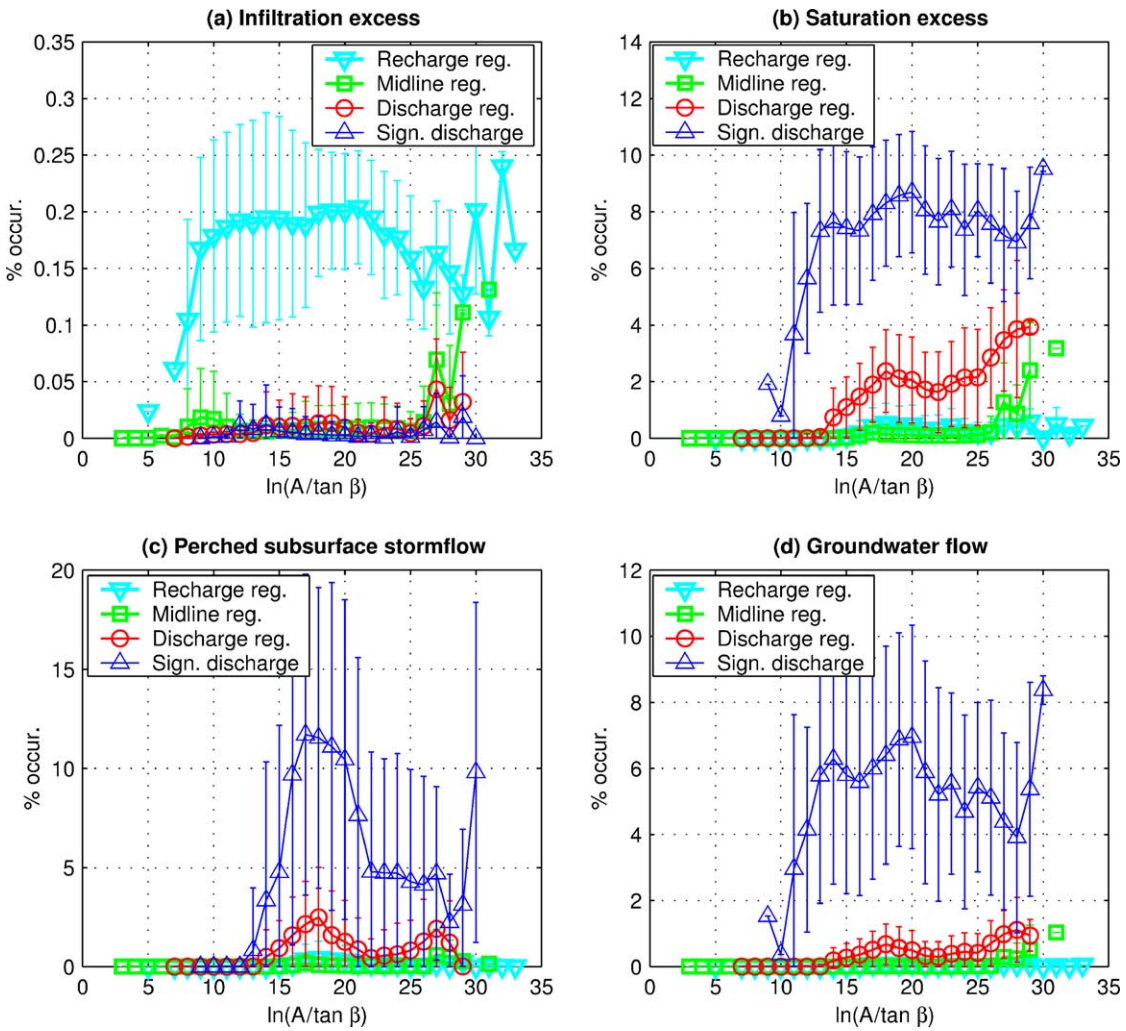

Fig. 22. Frequency of occurrence of runoff production events as percentage of the total simulation period 06/1993–07/2000 for different groundwater dynamics regions in relation to the topographic index, $\ln(A/\tan\beta)$, for the Blue River basin: (a) infiltration excess, (b) saturation excess, (c) perched subsurface stormflow, (d) groundwater flow.

Acknowledgements

This work was supported by the National Aeronautics and Space Administration (Contract NAG57475), National Oceanic and Atmospheric Administration (Contract NA97WH0033), and MIT—Office of Hydrology cooperative agreement. Authors thank the Office of Hydrology for initiation, support, and sponsoring the DMIP project.

Appendix A

1. Percent bias (PB, %):

$$\mathrm{PB} = \frac{\sum_{i=1}^{N}(S_i - O_i)}{\sum_{i=1}^{N} O_i} 100$$

2. Absolute percent bias (APB, %):

$$\mathrm{APB} = \frac{\sum_{i=1}^{N}|S_i - O_i|}{\sum_{i=1}^{N} O_i} 100$$

3. Observed or simulated mean streamflow, Q_{obs} and Q_{sim} (m^3/s):

$$\bar{Q} = \frac{\sum_{i=1}^{N} Q_i}{N}$$

4. Coefficient of variation of observed and simulated streamflow, C_{vobs} and C_{vsim}:

$$C_v = \frac{\sqrt{\frac{\sum_{i=1}^{N} (Q_i - \bar{Q})^2}{N-1}}}{\bar{Q}}$$

5. RMS error (%):

$$\mathrm{RMS} = \frac{\sqrt{\frac{\sum_{i=1}^{N} (S_i - O_i)^2}{N}}}{\bar{O}} 100$$

6. Absolute RMS error, (ARMS, m^3/s):

$$\mathrm{ARMS} = \sqrt{\frac{\sum_{i=1}^{N} (S_i - O_i)^2}{N}}$$

7. Correlation coefficient, R:

$$R = \frac{N\sum_{i=1}^{N} S_i O_i - \sum_{i=1}^{N} S_i \sum_{i=1}^{N} O_i}{\sqrt{\left[N\sum_{i=1}^{N} S_i^2 - \left(\sum_{i=1}^{N} S_i\right)^2\right]\left[N\sum_{i=1}^{N} O_i^2 - \left(\sum_{i=1}^{N} O_i\right)^2\right]}}$$

8. Nash-Sutcliffe coefficient, N_r:

$$N_r = 1 - \frac{\sum_{i=1}^{N} (S_i - O_i)^2}{N\bar{O}C_{vobs}}$$

S_i is the simulated discharge for each time step (m^3/s)
O_i is the observed discharge (m^3/s)
Q_i is either observed or simulated runoff (m^3/s)
$\bar{Q}$ is average observed or simulated runoff (m^3/s)
N is a total number of values within the time period of analysis.

References

Abbott, M.B., Bathurst, J.C., Cunge, J.A., O'Connell, P.E., Rasmussen, J., 1986a. An introduction to the European Hydrological System—Systeme Hydrologique European, 'SHE', 1: History and philosophy of a physically-based distributed modelling system. J. Hydrol. 87, 45–59.

Abbott, M.B., Bathurst, J.C., Cunge, J.A., O'Connell, P.E., Rasmussen, J., 1986b. An introduction to the European Hydrological System—Systeme Hydrologique Europeen 'SHE'. 2: Structure of a physically based, distributed modelling system. J. Hydrol. 87, 61–77.

Berger, K.P., Entekhabi, D., 2001. Basin hydrologic response relations to distributed physiographic descriptors and climate. J. Hydrol. 247(3–4), 169–182.

Beven, K., Calver, A., Morris, E.M., 1987. Institute of hydrology distributed model, Internal Report, Institute of Hydrology, Wallingford.

Bogaard, T.A., Van Asch, T.W.J., 2002. The role of the soil moisture balance in the unsaturated zone on movement and stability of the Beline landslide, France. Earth Surf. Proc. Lanforms 27(11), 1177–1188.

Bras, R.L., 1990. Hydrology: an Introduction to Hydrologic Science, Addison-Wesley/Longman, Reading, MA/London.

Carpenter, T.M., Sperfslage, J.A., Georgakakos, K.P., Sweeney, T., Fread, D.L., 1999. National threshold runoff estimation utilizing GIS in support of operational flash flood warning systems. J. Hydrol. 224(1–2), 21–44.

Carpenter, T.M., Georgakakos, K.P., Sperfslagea, J.A., 2001. On the parametric and NEXRAD-radar sensitivities of a distributed hydrologic model suitable for operational use. J. Hydrol. 253(1–4), 169–193.

Entekhabi, D., 2000. Land Surface Processes: Basic Tools and Concepts, Department of Civil and Environmental Engineering, MIT, Cambridge, MA.

Environmental Research Systems Institute, 1992. Understanding GIS: the Arc/Info Method, ESRI Press, Redlands, CA, 400 pp.

Finnerty, B.D., Smith, M.D., Seo, D.J., Koren, V.I., Moglen, G.E., 1997. Space-time scale sensitivity of the Sacramento model to radar-gage precipitation inputs. J. Hydrol. 203, 21–38.

Freeze, R.A., Cherry, J.A., 1979. Groundwater, Prentice Hall, Englwood Cliffs, NJ.

Garrote, L., Bras, R.L., 1995. A distributed model for real-time flood forecasting using digital elevation models. J. Hydrol. 167, 279–306.

Goodrich, D.C., Faurés, J.-M., Woolhiser, D.A., Lane, L.J., Sorooshian, S., 1995. Measurement and analysis of small-scale convective storm rainfall variability. J. Hydrol. 173, 283–308.

Grayson, R.B., Moore, I.D., McMahon, T.A., 1992. Physically-based hydrologic modelling, I, A terrain-based model for investigative purposes. Water Resour. Res. 28, 2639–2658.

Grayson, R.B., Bloschl, G., 2000. Spatial modelling of catchment dynamics. In: Grayson, R.B., Bloschl, G. (Eds.), Spatial Patterns in Catchment Hydrology: Observations and Modeling, Cambridge University Press, Cambridge, UK, pp. 51–81.

Hoeben, R., Troch, P.A., 2000. Assimilation of active microwave observation data for soil moisture profile estimation. Water Resour. Res. 36(10), 2805–2819.

Hu, Z., Islam, S., 1995. Prediction of ground surface temperature and soil moisture content by the force-restore method. Water Resour. Res. 31(10), 2531–2539.

Ivanov, V.Y., Vivoni, E.R., Bras, R.L., Entekhabi, D., 2004. Catchment hydrologic response with a fully-distributed triangulated irregular network model. Water Resour. Res. Submitted for publication.

Julien, P.Y., Saghafian, B., 1991. CASC2D User's Manual, Technical Report, Department of Civil Engineering, Colorado State University, Fort Collins.

Klemes, V., 1986. Operational testing of hydrological simulation models. Hydrol. Sci. J. - J. des Sci. Hydrol. 31(1), 13–24.

Koren, V.I., Finnerty, B.D., Schaake, J.C., Smith, M.B., Seo, D.J., Duan, Q.Y., 1999. Scale dependencies of hydrologic models to spatial variability of precipitation. J. Hydrol. 217(3–4), 285–302.

Leopold, L.B., Maddock, T., 1953. The Hydraulic Geometry of Stream Channels and Some Physiographic Implications, vol. 52. Geol. Surv. Profess. Paper. U.S. Gov. Print. Office, Washington.

Levine, J.B., Salvucci, G.D., 1999. Equilibrium analysis of groundwater-vadose zone interactions and the resulting spatial distribution of hydrologic fluxes across a Canadian prairie. Water Resour. Res. 35(5), 1369–1383.

Lin, J.D., 1980. On the force-restore method for prediction of ground surface temperature. J. Geophys. Res. 85(C6), 3251–3254.

McLaughlin, D., 1995. Recent developments in hydrologic data assimilation. Rev. Geophys. 33(Part 2), 977–984.

Monteith, J.L., 1965. Evaporation and environment. Symp. Soc. Exp. Biol. 19, 205–234.

Pauwels, V.R.N., Hoeben, R., Verhoest, N.E.C., De Troch, F.P., 2001. The importance of the spatial patterns of remotely sensed soil moisture in the improvement of discharge predictions for small-scale basins through data assimilation. J. Hydrol. 251(1–2), 88–102.

Pelletier, J.D., Malamud, B.D., Blodgett, T., Turcotte, D.L., 1997. Scale-invariance of soil moisture variability and its implications for the frequency-size distribution of landslides. Eng. Geol. 48(3–4), 255–268.

Penman, H.L., 1948. Natural evaporation from open water, bare soil and grass. Proceedings of the Society of London Series A193, 120–145.

Pessoa, M.L., Bras, R.L., Williams, E.R., 1993. Use of weather radar for flood forecasting in the Sieve river basin: a sensitivity analysis. J. Appl. Meteorol. 32(3), 462–475.

Poiani, K.A., Johnson, W.C., 1993. A spatial simulation model of hydrology and vegetation dynamics in semi-permanent prairie wetlands. Ecol. Appl. 3(2), 279–293.

Rawls, W.J., Brakensiek, D.L., Saxton, K.E., 1982. Estimation of soil water properties. Trans. ASAE 25(5), 1316–1330.

Rawls, W.J., Brakensiek, D.L., Miller, N., 1983. Green-ampt infiltration parameters from soils data. J. Hydraul. Eng. 109(1), 62–70.

Reed, S.M., Koren, V.I., Smith, M.B., Zhang, Z., Moreda, F., Seo, D.-J., et al., 2004. Overall distributed model intercomparison project results. J. Hydrol. 298(1–4), 27–60.

Refsgaard, J.C., 2000. Towards a formal approach to calibration and validation of models using spatial data. In: Grayson, R.B., Bloschl, G. (Eds.), Spatial Patterns in Catchment Hydrology: Observations and Modeling, Cambridge University Press, Cambridge, UK, pp. 329–354.

Reichle, R., Entekhabi, D., McLaughlin, D., 2001. Downscaling of radiobrightness measurements for soil moisture estimation. Water Resour. Res. 37(9), 1708–1718.

Rutter, A.J., Kershaw, K.A., Robins, P.C., Morton, A.J., 1971. A predictive model of rainfall interception in forests. 1. Derivation of the model from observation in a plantation of Corsican pine. Agric. Meteorol. 9, 367–384.

Rutter, A.J., Morton, A.J., Robins, P.C., 1975. A predictive model of interception in forests. 2. Generalization of the model and comparison with observations in some coniferous and hardwood stands. J. Appl. Ecol. 12, 367–380.

Salvucci, G.D., Entekhabi, D., 1995. Hillslope and climatic controls of hydrological fluxes. Water Resour. Res. 31, 1725–1739.

Schaake, J.C., Koren, V.I., Duan, Q.Y., Mitchell, K., Chen, F., 1996. Simple water balance model for estimating runoff at different spatial and temporal scales. J. Geophys. Res. Atm. 101(D3), 7461–7475.

Schellekens, J., Scatena, F.N., Bruijnzeel, L.A., Wickel, A.J., 1999. Modelling rainfall interception by a lowland tropical rain forest in northeastern Puerto Rico. J. Hydrol. 225(3–4), 168–184.

Schmugge, T.J., Kustas, W.P., Ritchie, J.C., Jackson, T.J., Rango, A., 2002. Remote sensing in hydrology. Adv. Water Resour. 25(8–12), 1367–1385.

Shuttleworth, W.J., 1979. Evaporation. Institute of Hydrology Report, no. 56, Wallingford, UK.

Sivapalan, M.K., Wood, E.F., Beven, K.J., 1987. On hydrologic similarity, 2, a scaled model of storm runoff production. Water Resour. Res. 23(12), 2266–2278.

Slack, J.R., Lumb, A.M., Landwehr, J.M., 2001. USGS Water-Resources Investigations Report, 93–4076.

Smith, M.B., Seo, D.-J., Koren, V.I., Reed, S., Zhang, Z., Duan, Q.-Y., Cong, S., Moreda, F., Anderson, R., 2004. The Distributed Model Intercomparison Project (DMIP): motivation and experiment design. J. Hydrol. 298(1–4), 4–26.

Taylor, A.H., Solem, M.N., 2001. Fire regimes and stand dynamics in an upper montane forest landscape in the southern Cascades, Caribou Wilderness, California. J. Torrey Botan. Soc. 128(4), 350–361.

Tucker, G.E., Lancaster, S.T., Gasparini, N.M., Bras, R.L., 2001. The channel-hillslope integrated landscape development (CHILD) model. In: Harmon, R.S., Doe, W.W. (Eds.), Landscape Erosion and Sedimentation Modeling, Kluwer Press, New York, pp. 349–388.

Vivoni, E.R., Ivanov, V.Y., Bras, R.L., Entekhabi, D., 2004. Generation of triangulated irregular networks based on hydrological Similarity. J. Hydrol. Eng. 9(4), 288–303.

Walker, J.P., Willgoose, G.R., Kalma, J.D., 2002. Three-dimensional soil moisture profile retrieval by assimilation

of near-surface measurements: simplified Kalman filter covariance forecasting and field application. Water Resour. Res. 38(12).

Wigmosta, M.S., Lance, W.V., Lettenmaier, D.P., 1994. A distributed hydrology—vegetation model for complex terrain. Water Resour. Res. 30(6).

Wooldridge, S., Kalma, J., Kuczera, G., 2001. Parameterisation of a simple semi-distributed model for assessing the impact of land-use on hydrologic response. J. Hydrol. 254(1–4), 16–32.

Wyss, J., Williams, E.R., Bras, R.L., 1990. Hydrologic modeling of New England river basins using radar rainfall data. J. Geophys. Res. 95(D3), 2143–2152.